A solid-state NMR and DFT study of compositional modulations in $Al_xGa_{1-x}As$†

Paulus J. Knijn,[a] P. Jan M. van Bentum,[a] Ernst R. H. van Eck,[a] Changming Fang,[a] Dennis L. A. G. Grimminck,[a] Robert A. de Groot,[a] Remco W. A. Havenith,[a] Martijn Marsman,[b] W. Leo Meerts,[a] Gilles A. de Wijs[a] and Arno P. M. Kentgens*[a]

Received 25th February 2010, Accepted 17th May 2010
DOI: 10.1039/c003624b

We have conducted ^{75}As and ^{69}Ga Nuclear Magnetic Resonance (NMR) experiments to investigate order/disorder in $Al_xGa_{1-x}As$ lift-off films with $x \sim 0.297$ and 0.489. We were able to identify all possible $As(Al_nGa_{4-n})$ sites with $n = 0$–4 coordinations in ^{75}As NMR spectra using spin-echo experiments at 18.8 Tesla. This was achieved by employing high rf field strengths using a small solenoid coil and an NMR probe specifically designed for this purpose. Spectral deconvolution, using an evolutionary algorithm, complies with the absence of long-range order if a CuAu based order parameter is imposed. An unconstrained fit shows a deviation of the statistics imposed by this type of ordering. The occupational disorder in the Ga and Al positions is reflected in a distribution of the Electric Field Gradients (EFGs) experienced at the different arsenic sites. We established that this can be modelled by summing the effects of the first coordination sphere and a Czjzek type distribution resulting from the compositional variation in the Al/Ga sub-lattice in the higher coordination spheres. ^{69}Ga 3QMAS and nutation data exclude the presence of highly symmetric sites and also show a distribution in EFG. The experimentally obtained quadrupolar interactions are in good agreement with calculations based on Density Functional Theory (DFT). Using additivity of EFG tensors arising from distant charge perturbations, we could use DFT to model the EFG distributions of the $n = 0$–4 sites, reproducing the Czjzek and extended Czjzek distributions that were found experimentally. On the basis of these calculations we conclude that the ^{75}As quadrupolar interaction is sensitive to compositional modulations up to the 7th coordination shell in these systems.

Introduction

Thin film semiconductors are of great importance for electronic and photonic devices. The development of new or improved devices relies on a detailed knowledge of the structural properties of the materials. In this respect compositional modulation and ordering play an important role. As was predicted by Zunger and coworkers[1] in the mid eighties, long-range order can occur in semiconductor alloys with size-mismatched constituents, despite the fact that the mixing enthalpy is positive. This can be explained by the fact that the statistical average over the many different local environments is positive, because some of these clusters are strained. Periodically repeating a three-dimensional geometric re-arrangement can minimize strain and leads to long-range order. These predictions were soon verified by experimental observations of ordering in semiconductors by Stringfellow and coworkers[2] and Gomyo and Suzuki.[3] For many III–V compounds the ordered phase has positive excess enthalpy, these structures can order metastably in bulk and can become stable in epitaxially grown films. Other crystallographic arrangements such as the CuPt structure do not possess enough geometrical degrees of freedom to permit all chemical bonds to attain their ideal length, and are therefore unstable. Nevertheless, ordering of alternating diagonal planes in the ⟨111⟩ direction was found experimentally which was explained by assuming atomic dimerization at the surface, inducing CuPt ordering in the subsurface layers.[4]

As there is hardly any size-mismatch in AlGaAs, long-range order has not been widely observed. Nevertheless, Krahmer *et al.*[5] reported evidence of a direct–indirect conduction band transition for $x = 0.4$ in $Al_xGa_{1-x}As$ by using reflectance anisotropy spectrometry, indicating an increase in order. They report that doping, temperature and substrate orientation all affect the anisotropy of the lattice, but did not quantify this in terms of an order parameter. X-ray measurements from Kuan[6] *et al.* reported a low long-range order parameter $S < 0.5$ for $Al_{0.75}Ga_{0.25}As$ grown by MOCVD, depending on growth conditions. More recent X-ray measurements by van Niftrik *et al.*[7] indicated a lower long-range ordering of $S \leq 0.05$ for $Al_{0.5}Ga_{0.5}As$ and $S \leq 0.06$ for $Al_{0.25}Ga_{0.75}As$. Despite the prediction of almost no long-range ordering with X-ray, studies of the local interface for dilute AlGaAs with cross-sectional STM (XSTM) indicate the appearance of short

[a] *Institute for Molecules and Materials, Radboud University Nijmegen, Toernooiveld 1, NL-6525 ED Nijmegen, The Netherlands*
[b] *Institut für Materialphysik and Centre for Computational Materials Science, Universität Wien, A 1090, Wien, Austria*

† Electronic supplementary information (ESI) available: Additional information including an experimental NMR section concerning the QCPMG data and a theoretical DFT part. See DOI: 10.1039/c003624b

strings. In 1994, an XSTM study by Smith *et al.*[8] confirmed that an interrupted growth process can create short period super lattices in AlGaAs. In 1996, Smith *et al.*[9] noticed a small deviation from random ordering in the Al–Al pair distributions at the interface of GaAs and $Al_{0.05}Ga_{0.95}As$. In 1999, Heinrich *et al.*[10] clearly observed strings of Al atoms in the GaAs matrix, up to five atoms in MOVPE grown $Al_{0.15}Ga_{0.85}As$ along low indexed crystallographic directions.

In general, the composition of III–V semiconductors is difficult to describe since various structural features can exist (simultaneously) at different length scales. For instance, the presence of both ordered and disordered domains makes it hard to analyze these structures in detail. The degree of order will affect many physical and electronic properties such as electronic transport, mobility, thermodynamic stability and electro-optical properties. Many properties of AlGaAs are described in detail in the work of Adachi.[11] Considering the limited number of reports on long-range order in AlGaAs thin films as studied by diffraction techniques, whereas specific ordered structures are seen in a number of microscopic observations, it is interesting to study these materials with a complimentary method such as NMR. As NMR probes short-range order, the presence of locally occurring structures can be detected if present in sufficiently high concentrations. Since the NMR signal is composed out of contributions from the entire sample, the possibility that one is studying a specific anomaly is reduced. Long-range ordered structures will result in a specific signature which can be directly distinguished from a disordered structure.

NMR is a versatile technique that in principle can detect all nuclei which possess a spin through their interaction with an external magnetic field (the Zeeman interaction). A number of interactions make NMR useful as they give the spectra a specific appearance which can be related to local structure and dynamics of the material under study. In the present work two of these are important; the chemical shift and the quadrupolar interaction. The external magnetic field used in NMR induces local fields in molecules and materials that modify the resonance frequencies and makes different sites distinguishable, this is referred to as the chemical shift. For a $I > 1/2$ nucleus, the quadrupolar interaction arises from the presence of an electric field gradient (EFG), resulting from the local charge distribution around the site of a nucleus which interacts with the non-spherically symmetric charge distribution of that nucleus. Although NMR is an appealing technique that may form a bridge between diffraction studies and microscopic observations in the study of III–V semiconductors, there are a number of challenges that have to be addressed. Many nuclei encountered in III–V semiconductors are quadrupolar nuclei, possessing a large quadrupolar moment $e{\cdot}Q$. The strength of the interaction expressed through the quadrupole coupling constant $C_q = e^2qQ/h$ can be very large, easily in the tens of MHz regime. Although this interaction can still be treated as perturbation of the Zeeman Hamiltonian, if sufficiently high external fields are applied, the quadrupolar interaction has, in general, to be treated as a second-order perturbation. To first-order the spectral features of the so-called satellite transitions are dispersed over a wide frequency range of the order of $\nu_q = 3C_q/(2I(2I - 1))$ whereas the shape of the observed patterns reflects the asymmetry parameter η of the interaction. The central transition, $\langle 1/2;-1/2\rangle$ is not affected by the quadrupolar interaction in first order but the second-order features are dispersed over a frequency range of the order of ν_q^2/ν_0, where the shape is again characteristic for the asymmetry of the EFG tensor. Even at high external fields this second-order interaction can result in MHz bandwidths for nuclei such as ^{75}As. To excite such a bandwidth efficiently, sufficiently large rf field strengths are needed. In relation to this one has to realize that the behavior of the spin system in the rotating frame during rf-irradiation depends on the ratio of the quadrupolar frequency and the rf field strength.[12,13] Therefore, the effective excitation of the spin systems has to be modeled accurately, especially when quantitative results of different spin systems with widely differing quadrupolar parameters are needed. Additionally, with such different sites present spectral overlap will often occur, demanding a robust approach to spectral deconvolution. Finally, to interpret NMR spectra in relation to structures, a first principle approach such as DFT is desirable.

In the present contribution we address all of the issues described above. Using small rf-coils it is possible to generate appropriate rf-fields to excite a broad bandwidth. These coils also help in overcoming the sensitivity problems related to the study of thin film materials leading to very low quantities of sample material.[14] Here we compare spin-echo experiments and frequency-stepped Quadrupolar Carr–Purcell–Meiboom–Gill (QCPMG)[15–18] experiments to obtain static ^{75}As spectra of two AlGaAs films with different composition. Spectral deconvolution and quantification of the spectra is addressed with a dedicated program based on an evolutionary algorithm. ^{69}Ga 3QMAS[19] and nutation[12,13] NMR spectra have been obtained to gain complementary information about the local symmetry of the different lattice sites. Although this work focuses on AlGaAs thin film materials, the approach presented can be applied for the investigation of compositional modulations in most III–V semiconductors and materials with related variations in the occupancy of different lattice positions, sometimes called substitutional disorder.

Furthermore, we develop a modeling approach to accurately describe the EFG distributions of various kinds of sites. To this end we extended the first-principles DFT code of VASP (Vienna *Ab initio* Simulation Program), to calculate EFGs and build a model wherein we can quickly calculate the EFGs for several millions of configurations based on just one DFT calculation. This model is used to estimate the sensitivity of EFGs to variations in the order parameter. It has a wider scope, as it in principle provides the capability to quickly obtain electronic density distributions for any structural model for any ''random'' alloy with fixed sub-lattices.

Studying (dis-)order with NMR

Based on theory used to analyze diffraction data, an order parameter S can be defined to quantify the degree of long-range order related to the fractional occupancy of lattice

sites by their preferred atom.[6] $S = 0$ represents a completely random structure and $S = 1$ corresponds to a completely ordered lattice:

$$S = |r_A + r_B - 1|, \quad (1)$$

where r_A and r_B are the fractions of A and B lattice sites that are occupied by their preferred atom. For binary systems, as considered here, this means that $1 - r_A$ constitutes the fraction of A lattice sites occupied by B atoms and $1 - r_B$ the fraction of B sites occupied by A atoms. In case of random occupation of the lattice sites, *i.e.* the absence of ordering, $r_A = x$ and $r_B = 1 - x$. For (partially) ordered structures the fractional occupancy of the A and B sites by their preferred atoms can be re-written as:

$$r_A = x + S/2 \quad (2)$$

$$r_B = (1 - x) + S/2 \quad (3)$$

Using this definition we should realize that the order parameter S can reach a value of $2x$ at most. A perfectly ordered structure can only be achieved for $x = 0.5$. S can be scaled, however, so that the maximum possible order for any given composition x gives an order parameter $S = 1$.[20]

The presence of (dis-)order in a structure is in most cases manifested in quantifiable NMR parameters. Different structural environments in a material can be distinguished based on the NMR interactions which are influenced by the different coordinating atoms. For example, Tycko *et al.*[22] distinguished five ^{31}P sites in the ^{31}P MAS NMR spectrum of GaInP. These five resonances were assigned to the different phosphorus nearest neighbors coordinations P[$In_{4-n}Ga_n$] with $n = 0$–4. The sites are resolved in this spectrum due to their different isotropic chemical shifts. The presence of order in the sample is reflected in the statistics of the occurrence of the various coordinations.[21,22] The probabilities p_n for the occupations of the C[A_nB_{4-n}] sites are

$$\begin{aligned} p_0 &= p_{C[B_4]} \\ p_1 &= p_{C[A_1B_3]} \\ p_2 &= p_{C[A_2B_2]} \\ p_3 &= p_{C[A_3B_1]} \\ p_4 &= p_{C[A_4]} \end{aligned} \quad (4)$$

Here, two types of ordering are considered for $A_xB_{1-x}C$ type materials, see Fig. 1. CuPt ordering, with diagonal planes, stacked in the ⟨111⟩ direction or a CuAu, with alternating planes in ⟨001⟩. For each configuration, we can quantify the probability of their occurrence. The 16 possible atomic configurations in the first shell contribute each with a different probability:

$$p_0^{CuPt} = \tfrac{1}{2}r_B(1 - r_A)^3 + \tfrac{1}{2}(1 - r_A)r_B^3$$

$$p_1^{CuPt} = \tfrac{1}{2}(1 - r_B)(1 - r_A)^3 + \tfrac{1}{2}r_Ar_B^3 + \tfrac{3}{2}r_Ar_B(1 - r_A)^2 + \tfrac{3}{2}(1 - r_B)(1 - r_A)r_B^2$$

$$p_2^{CuPt} = \tfrac{3}{2}(1 - r_B)r_A(1 - r_A)^2 + \tfrac{3}{2}r_A(1 - r_B)r_B^2 + \tfrac{3}{2}(1 - r_B)^2r_B(1 - r_A) + \tfrac{3}{2}r_A^2(1 - r_A)r_B$$

$$p_3^{CuPt} = \tfrac{1}{2}r_A^3r_B + \tfrac{1}{2}(1 - r_B)^3(1 - r_A) + \tfrac{3}{2}r_A^2(1 - r_B)(1 - r_A) + \tfrac{3}{2}(1 - r_B)^2r_Ar_B$$

$$p_4^{CuPt} = \tfrac{1}{2}(1 - r_B)r_A^3 + \tfrac{1}{2}r_A(1 - r_B)^3 \quad (5)$$

$$p_0^{CuAu} = (1 - r_A)^2r_B^2$$

$$p_1^{CuAu} = 2r_A(1 - r_A)r_B^2 + 2(1 - r_B)(1 - r_A)^2r_B$$

$$p_2^{CuAu} = r_A^2r_B^2 + (1 - r_B)^2(1 - r_A)^2 + 4r_A(1 - r_B)r_B(1 - r_A)$$

$$p_3^{CuAu} = 2r_A^2(1 - r_B)r_B + 2r_A(1 - r_B)^2(1 - r_A)$$

$$p_4^{CuAu} = (1 - r_B)^2r_A^2 \quad (6)$$

As the probabilities correspond to the integrated peak intensities of the different sites, one can determine the long-range order parameter by drawing the experimental peak intensities in a plot of calculated intensities *versus* order parameter S. Using the relative ^{31}P peak intensities Tycko *et al.*[22] were able to set an upper limit of $S < 0.6$ for the CuPt type ordering in InGaP. Degen *et al.*[21] observed the ^{75}As resonances of the locally symmetric As[Al_4] and As[Ga_4] coordinations in static single-pulse excitation experiments on powdered AlGaAs films. They were able to set an upper limit of $S < 0.2$ and $S < 0.4$ for CuAu and CuPt ordering respectively. Although spin-echo experiments hinted at the presence of the other ^{75}As coordinations, these proved to be too broad to be efficiently excited and resolved in the spectrum.

Finding low values for the long range order parameter S indicates that the atomic distribution of A and B atoms becomes more or less random over their lattice positions. It may well be, however, that there is still a preference for *local*

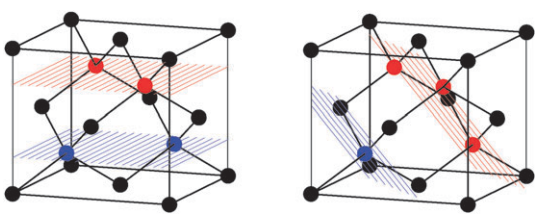

Fig. 1 Order in the face centered cubic lattice structure of AlGaAs. The black atoms are Arsenic, the other atoms are the Al and Ga cations. *left* 2-fold symmetry of the As nucleus for a $AsAl_2Ga_2$ configuration, CuAu ordered with planes alternating along the ⟨001⟩ direction. *right* 3-fold tetrahedral symmetry of the As nucleus for a $AsAl_3Ga$ and $AsAlGa_3$ configuration, also called CuPt ordered lattice with planes extending along the ⟨111⟩ direction. Coordination numbers and distances are 0.40 and 0.245 nm for the first coordination sphere, 1.20 and 0.40 nm for the second coordination sphere and 1.20 and 0.469 nm for the third coordination sphere. The lattice constant is $A_x = 0.566140 - 0.000809 \cdot x$ nm.[21]

ordering of Al and Ga in the sample, *e.g.*, when A atoms prefer B atoms in their vicinity and *vice versa*. Alternatively, atoms can show a tendency to be close neighbors which is referred to as clustering. Short-range ordering and clustering is very difficult to detect with diffraction techniques as they cause only very weak diffuse scattering. In NMR the statistics of the different coordinations will be modulated by either short range order or clustering, which should be expressed in increased numbers for p_0 or p_4. The exact effect and size of the variations will depend on the scale and abundance of the locally ordered structures and may be difficult to interpret depending on the accuracy with which the spectral line intensities can be determined.

Besides modulating the intensities of the various $C[A_nB_{4-n}]$ resonances in the spectra it should be realized, however, that the distribution of A and B atoms over the lattice also affects the NMR parameters such as the chemical shift and the quadrupolar interaction parameters ν_q and η of these sites. Especially for the quadrupolar interaction it is important to consider that the interaction is not fully determined locally. Although the electric field gradient tensor is dominated by the first shell bonds, further coordination shells still have a distinct influence. This is witnessed by the fact that the symmetric first shell As coordinations, $As[Al_4]$ and $As[Ga_4]$, observed by Degen *et al.*[21] in AlGaAs, show non-zero quadrupolar interactions with quadrupolar coupling constants of 800 and 600 kHz respectively.

Structural disorder leads to distributions in chemical shift and quadrupolar interactions, which affect the measured line shapes in a characteristic way. Therefore, a detailed study of the line shapes in disordered solids can be interpreted in terms of structural variations in these materials if one can extract the probability density function for the quadrupolar interaction parameters from the spectra *and* compute the EFG tensors for a given structure, *e.g.*, based on first principles DFT based calculations.

Extraction of the probability density function from NMR spectra of randomly oriented powder samples is not trivial as the distribution in quadrupolar NMR parameters is convoluted with the powder averaging over all possible tensor orientations in the ensemble. In the NMR literature several approaches to model the probability density function(s) for the quadrupolar interaction parameters can be found. The most basic approach is to assume Gaussian distributions in C_q and η. Although such distributions are not physically justified they regularly do produce line shapes similar to the experimental ones and can therefore be used in spectral deconvolutions in order to properly quantify the relative line intensities. One should be careful with interpreting these results in terms of structural disorder, however, especially where the asymmetry parameter η is concerned. First of all, the structural parameters are not additively described by quadrupolar parameters and are therefore not expected to be normally distributed and moreover ν_q and η are coupled as they both depend on the local electronic coordination around a nucleus. Jäger *et al.*[23] and Meinhold *et al.*[24] have improved on this basic model by assuming normal distributions in the eigenvalues of the EFG tensor and applying constraints to warrant the tracelessness of this tensor. Again good line shapes can be obtained but this approach is still not satisfactory as C_q and η are treated independently, needing a starting value for η. Moreover, the distribution is generated numerically lacking an analytical description.

A physically more sound model for describing the distribution of electric field gradients in amorphous solids has been developed by Czjzek *et al.*[25] They proposed a joint probability density function

$$P(V_{zz},\eta) = A \cdot \exp\left(\frac{-V_{zz}^2(1+\eta^2/3)}{2\sigma^2}\right)$$
$$A = \frac{V_{zz}^{d-1} \cdot \eta(1-\eta^2/9)}{\sqrt{2\pi}\sigma^d}, \quad (7)$$

in which the average quadrupolar coupling constant depends on σ and d, see Table 1. In this work, we show that for a randomly ordered lattice, the quadrupolar distributions caused by a random occupancy of the A and B sites over the lattice can be described by a Czjzek distribution with $d = 5$ for the symmetric $C[A_4]$ and $C[B_4]$ sites. These distributions are isotropic and rotation invariant. Eqn (7) is derived from the fact that the real terms $U_m (m = 0–4)$ (defined in references)[25,26] of the EFG tensor are independently, normally distributed variables for amorphous solids with random ionic coordinations. The five independent spherical tensor elements $V_{i,k}$ of the EFG tensor are linear combinations of these U_m. A similar approach was introduced by Stöckmann[27] describing the effect of randomly distributed defects in cubic crystals.

As was outlined by Massiot and coworkers,[28] the Czjzek distribution can only be used if the number of structural elements contributing to the EFG is sufficiently large, meaning that for a given coordination shell the coordination number should be large. This will in general not be the case for the first coordination shell. Therefore the Czjzek distribution can in principle only be used if the first coordination sphere hardly contributes to the EFG as is the case for the symmetric $As[Al_4]$ and $As[Ga_4]$ sites in AlGaAs or the octahedrally and tetrahedrally coordinated aluminium sites discussed by Massiot *et al.*[28] Clearly, the first coordination sphere dominates the EFG for the asymmetric $As[Al_nGa_{4-n}]$ sites with $n = 1,2,3$ in AlGaAs. To deal with this situation an extension of the Czjzek approach is needed, considering the case of an EFG contribution of a well-defined local coordination of a given atomic species and adding to that the effect of disorder of more remote atomic shells and possible other random contributions to the total EFG. Due to the good lattice matching of the

Table 1 The ratio of the average $\langle V_{zz}\rangle$ to the σ in a Czjzek distribution as a function of the power factor d obtained by integrating eqn (7) over all η for a given σ

d	$\langle V_{zz}\rangle/\sigma$
1	0.74
2	1.17
3	1.49
4	1.76
5	2.00

AlGaAs lattice, we neglect any stress in the lattice and propose to use additivity for the local and remote contributions to these EFGs. This is implemented numerically by adding the (fixed) contribution of the first coordination shell to the Czjzek distribution resulting from (random) occupancy of Al and Ga lattice sites in the further coordination shells. First, the principal EFG tensor values are generated from the Czjzek distribution using $V_{xx} = -V_{zz}(\eta+1)/2$ and $V_{yy} = V_{zz}(\eta - 1)/2$. The resulting tensor V is then rotated over a set of Euler angles using $V_{rot} = R(\alpha, \beta, \gamma)^{\bullet} V^{\bullet} R(\alpha, \beta, \gamma)^{T}$, with R^T the transposed rotation matrix. The relative orientation is randomized by taking all possible orientations into account. The first shell EFG is added to this tensor after which it is diagonalized and sorted using $V_{zz} \geq V_{xx} \geq V_{yy}$. The final distribution is generated by integration over all possible angles on a sphere ensuring the isotropic character of the distribution. The resulting V_{zz} and η values are placed on a new grid with the weights of the original Czjzek distribution. For Al_2Ga_2, the first shell tensor $V(0)$ is defined by a single scalar value $V^{\eta 1}$ and $\eta(0) = 1$

$$V = \begin{bmatrix} -V^{\eta 1} & 0 & 0 \\ 0 & 0 & 0 \\ 0 & 0 & V^{\eta 1} \end{bmatrix} \quad (8)$$

The first shell tensor of a Al_1Ga_3/Al_3Ga_1 site is defined by $V^{\eta 0}$ and $\eta(0) = 0$

$$V = \begin{bmatrix} -V^{\eta 0}/2 & 0 & 0 \\ 0 & -V^{\eta 0}/2 & 0 \\ 0 & 0 & V^{\eta 0} \end{bmatrix} \quad (9)$$

The "extended Czjzek" distribution generated in this way coincides with the extended Gaussian Isotropic Model (GIM) introduced by Le Caër and Brand.[26] These authors give an in-depth and general discussion of models for the distributions of electric field gradients in disordered solids. Their extended Gaussian Isotropic Model (GIM) considers the case of an EFG tensor V_0 added to a random tensor background contribution $\tilde{V}_{GI}$ with a ratio y, $\tilde{V} = (1 - y)\cdot V_0 + y\cdot \tilde{V}_{GI}$. Here we assign $y = 0.5$, since there is an equal contribution of the EFG tensor from the higher coordination spheres and the first coordination shell. Since a normalization is missing, it is more convenient to consider $\tilde{V} = V_0 + \tilde{V}_{GI}$. Le Caër and Brand describe the quadrupolar distribution by an exponential expression of three terms, integrated over a sphere, see ref. 26, using the Euler angles α, β, γ. This equation is slightly modified here into eqn (10). The nominator of the exponent consists of a mix term $\vec{U}'\cdot\vec{U}(0)$, an offset term which is constant $V_{zz}(0)^2\cdot(1 + \eta(0)^2/3)$ and merely scales the intensities and a Czjzek term $V_{zz}^2\cdot(1 + \eta^2/3)$. The "ordered" first shell tensor has magnitude $V_{zz}(0)$ and an asymmetry parameter $\eta(0)$. In comparison with $\eta(0) = 0$, there are two additional cross-terms in $\vec{U}'\cdot\vec{U}(0)$, when $\eta(0) = 1$. Even though the offset term is constant, as the ratio V_{zz}/σ can become large, all exponential terms need to be placed inside the integral and cannot be placed in front, since individually the exponential terms can become extremely large $>10^{700}$ in case of a strong first shell tensor $V_{zz}(0) > 40 \times 10^{20}$ V m^{-2}.

$$f(V_{zz}, \eta) \propto A \cdot \iint \exp\left(\frac{\tilde{U}'\cdot\tilde{U}'(0)}{2\sigma^2} - \frac{V_{zz}(0)^2\cdot(1+\eta(0)^2/3) - V_{zz}^2\cdot(1+\eta^2/3)}{2\sigma^2}\right) d\alpha \sin(\beta) d\beta d\gamma$$

$$\vec{U}'\cdot\vec{U}'(0) = 2\cdot V_{zz}\cdot\left(V_{zz}(0)a_{11} + \frac{\eta(0)V_{zz}(0)a_{15}}{\sqrt{3}}\right) + \frac{2\cdot\eta V_{zz}}{\sqrt{3}}\left(V_{zz}(0)a_{51} + \frac{\eta(0)V_{zz}(0)a_{55}}{\sqrt{3}}\right), \quad (10)$$

with $A_{ij}(\alpha, \beta, \gamma)$ as defined in ref. 26 and A as in eqn (7). For $\eta(0) = 0$ this equation can be written into a modified Bessel function form (see eqn 61 in ref. 26). Practically, the (V_{zz}, η) distribution for $\eta(0) = 0$ showed good overlap with the previous equation in a simplified, approximated form without integral

$$f(V_{zz}, \eta) \sim A\cdot\exp\left(\frac{V_{zz}\cdot V_{zz}(0)}{2\sigma^2} - \frac{-V_{zz}(0)^2\cdot(1+\eta(0)^2/3) - V_{zz}^2\cdot(1+\eta^2/3)}{2\sigma^2}\right) \quad (11)$$

allowing a much faster calculation. The only difference with the extended Czjzek distribution that was introduced previously, is the scaling of the tensor terms and the extra y parameter. Although Le Caër and Brand[26] use y as a parameter for local ordering (crystalline, mixed or random domains), we consider this effect simply by adjusting the magnitude of the first shell tensor $V(0)$, omitting the need for an extra variable in this approach. Substituting $V(0) = 0$ corresponds to the original Czjzek distribution. Very recently Le Caër and coworkers have further developed their extension of the Czjzek model in view of an application to ^{71}Ga NMR spectra of chalcogenide glasses.[29]

A final important step for interpreting distributions in quadrupolar NMR parameters is being able to predict the quadrupolar parameters on the basis of a given structural model. The calculation of EFGs using Density Functional theory (DFT) has been implemented in the Full Potential Linearised Augumented Plane Wave (FLAPW) method by Herzig *et al.*[30] and in the PAW (Projector Augmented Wave) method by Petrilli *et al.*[31] Following the latter we implemented the EFG calculation in the first-principles electronic structure program VASP (Vienna *Ab initio* Simulation Package).[32–35] An additional challenge in this context is to appropriately model the effects of the structural variations present in the material. In case of AlGaAs, however, the effects of local charge (re)distributions arising from single lattice modifications are additive, so that various disordered configurations can be modeled with relatively low computational cost.

Experimental

Sample preparation

The AlGaAs samples were grown by Metal Organic Vapor Phase Epitaxy. Undoped 2 inch GaAs wafers with crystal orientation ⟨100⟩, 15 degrees off towards ⟨111⟩ were used as substrates. A typical sample consisted of a 15 nm Si-doped AlAs buffer and a 5 μm undoped $Al_xGa_{1-x}As$ layer. A growth series with nominal aluminium fractions of $x = 0$, 0.297 was produced. A sample with $x = 0.489$ was grown on a substrate 2 degrees off towards ⟨110⟩. An epitaxial lift-off process[36] was applied to separate the $Al_xGa_{1-x}As$ layer from the substrate by selectively etching the intermediate Si-doped AlAs layer with a hydrogen fluoride solution. The $Al_xGa_{1-x}As$ thin films (≈mg quantities) were crushed into a powder with a typical grain size of a few micrometres and subsequently transferred to plastic sample holders for NMR measurements. The sample holders were made of PolyEtherEtherKeton (PEEK).

NMR experiments

A home-built, static XH probe operating at 137 MHz for arsenic (18.8 T) was designed for achieving high rf fields. The coil was a 5-turn solenoid with a 1.2 mm internal diameter, made of a silver-plated, 220 μm diameter wire. The sample space was confined to a length of 2 mm and a diameter of 0.6 mm. The Q factor of the probe was determined to be ≈38. Two Allen-Bradley 1 kΩ high power resistors were put parallel to the tuning capacitor to reduce the Q factor to ≈ 20 to allow frequency-stepped experiments without retuning the probe. The rf-field strength was determined by obtaining ^{75}As nutation spectra from a sample of GaAs. In this sample As occupies a cubically symmetric lattice and therefore the signal nutates with frequency ν_{rf}. rf field strength up to 800 kHz were achieved using approximately 800 Watts of power. In the QCPMG and Hahn-echo pulse experiments very short pulses are used so one has to take into account that the maximum voltage is never reached due to the pulse rise time depending on the Q factor of the probe (see supplementary material). Therefore actual rf fields amounted to 390 kHz and 625 kHz in the QCPMG and Hahn-echo experiment respectively.

I. ^{75}As QCPMG. A well-established experiment for acquiring very wide-line spectra with high sensitivity is the frequency-stepped QCPMG experiment.[15–18] For such an experiment it is useful to reduce the probes' Q factor (here to 20). The flat response of the probe minimizes the phase variations as a function of frequency. This is advantageous since the probe does not need to be re-tuned and the intensity loss at large frequency offsets is almost negligible. 24 respectively 22 experiments were performed at 18.8 T using a Varian InfinityPlus console. The frequency step size was 125 kHz covering a spectral width of 3 MHz for $Al_{0.297}Ga_{0.703}As$ and $Al_{0.489}Ga_{0.511}As$. The $x \approx 0.297$ spectrum was recorded with 10.000 scans and the $x \approx 0.489$ with 5.400 scans at each frequency step. Because T_2 is long, the number of echoes acquired (242) was limited by experimental limitations (121.000 data points in 30 ms). The 90° and 180° pulse times were 0.32 μs and 0.64 μs respectively. A repetition delay of 1 s was used, acquiring a spectral width of 4 MHz. Each echo acquisition time was 125 μs with 7.5 μs experimental delay before and after the 180° pulse of each echo. The individual 500 point whole-echos were T_2 weighted before co-adding, and subsequently swapped around the echo maximum and Fourier transformed. A more detailed description of acquisition and processing of the QCPMG data is given in the supplementary material.

II. ^{75}As Hahn-echo. Hahn-Echo experiments were obtained at 18.8 T, corresponding to a ^{75}As frequency of 136.93 MHz, using a Varian InfinityPlus Console $\left(\frac{\pi}{2}^{x,-x} - \tau_1 - \pi^{-y} - \tau_2 - \mathrm{ACQ}^{x,-x}\right)$. A recycle delay of 1 s was employed. Whole echoes were recorded which were processed by swapping the data around the echo maximum followed by apodization (exponential) and zero-filling to 8192 points before Fourier transformation. The spectral width was 5 MHz. The $x \approx 0.297$ Hahn-echo spectrum was acquired with 75.000 scans and echo times of $\tau_1 = 200$ μs, $\tau_2 = 75$ μs and 25 μs delay from the acquisition and receiver delay. The 90° and the 180° pulse times were 0.2 μs respectively 0.4 μs. 166.000 scans were averaged in the $x \approx 0.489$ Hahn-echo data with $\tau_1 = 175$ μs, $\tau_2 = 5$ μs and 20 μs delay from the acquisition and receiver delay.

III. ^{69}Ga Nutation and 3QMAS. A series of ^{69}Ga static nutation spectra using different rf-field strengths were obtained for $Al_{0.297}Ga_{0.703}As$ at 14.1 T on a Chemagnetics Infinty 600 MHz spectrometer. The same probe was used for these experiments, tuned to 143.99 MHz with a Q factor of ~50. A z-filtered ^{69}Ga 3QMAS spectrum, using hyper-complex States TPPI,[37] was recorded at 9.4 T, 96.013087 MHz, on a Chemagnetics Infinity 400 MHz spectrometer. Here a spinning speed of 15 kHz was employed, using a Chemagnetics 2.5 mm HX probe.

IV. Spin–lattice relaxation times. To ensure quantitative evaluations of the spectra, spin–lattice relaxation times were determined for $Al_{0.297}Ga_{0.703}As$ using saturation recovery experiments, as summarized in Table 2. The values for this $x \approx 0.297$ composition do not differ strongly from the values determined earlier[21] for a sample with composition $Al_{0.498}Ga_{0.511}As$, indicating no significant changes in relaxation mechanism for different compositions. The T_1 of ^{75}As in bulk GaAs was 0.33 ± 0.05 s.

Spectral deconvolution

An important objective of this study is to characterize the ^{75}As coordinations in $Al_xGa_{1-x}As$ and determine their relative intensities. The analysis can become complex due to the presence of several overlapping resonances with a distribution in NMR interaction parameters. Here we resort to fitting

Table 2 T_1(s) relaxation times obtained using saturation recovery at 14.1 Tesla

	$Al_{0.297}Ga_{0.703}As$	$Al_{0.489}Ga_{0.511}As$[21]
^{69}Ga	—	0.77±0.04
^{71}Ga	0.11±0.04	0.15 ± 0.08
^{27}Al	18 ± 1	16.1 ± 0.4
^{75}As	0.27 ± 0.02	0.28 ± 0.03

procedures based on an evolutionary algorithm to provide knowledge about intensities, NMR parameters and their distribution, and the associated error margins. The program is based on the work by Meerts[38] and will be described in detail in a forthcoming publication. The algorithm uses a library database of time domain data sets which were generated using SIMPSON.[39,40] In this way the experimental conditions can be mimicked accurately for each experiment. For each site a group of simulated data sets are added to describe a distribution in interaction parameters. The weight of each set is determined by the selected distribution function, *e.g.*, given by the work of Czjzek[25] and Le Caër and Brand.[26] For the Hahn-echo spectra, approximately 1600 datasets were generated based on the experimental rf-field strength and bandwidth. In the simulations, the maximum of the echo was recorded to identify the intensity contribution for each site. For the QCPMG spectra a slightly different approach was followed. Calculating all echoes in a QCPMG experiment for each quadrupolar interaction is too time consuming and therefore only a single echo was calculated assuming ideal pulses. Each subset was Fourier transformed into five absolute simulated spectra with ideal lineshapes but including quadrupolar distributions, which were least square fitted to the absolute, experimental spectrum. To cover all values appearing in the spectra, the quadrupolar interaction parameters of the As[Ga_4] and As[Al_4] site were varied over a range of $0 \leq \eta \leq 1$, $0 \leq C_q \leq 2$ MHz while the As[Al_2Ga_2] site had a range of $0.9 \leq \eta \leq 1$, $31 \leq C_q \leq 35$ MHz and the As[Al_1Ga_3] and As[Al_1Ga_3] site $0 \leq \eta \leq 0.1$, $31 \leq C_q \leq 35$ MHz. In all fits, the cost function was calculated using a normalized, least square summation

$$\chi^2 = \sum_{i=1}^{n} \left(\frac{f_i}{f_{\max}} - \frac{g_i}{g_{\max}} \right)^2, \qquad (12)$$

here f is the experimental spectrum and g the calculated spectrum from the library and n the number of points. The calculations were performed using up to 20 nodes of a high speed cluster based on Sunfire X4100 computers.

Density functional theory

Electronic structure calculations were carried out to relate quadrupolar interaction parameters to the different cation configurations. The local electric field gradients have been calculated with the first-principles molecular-dynamics programme VASP,[32–35] using density functional theory and the PAW method[41,42] following the approach by Petrilli *et al.*[31] several convergence tests were carried out, in particular to estimate the effect of the semi-core states and compared with state-of-the-art quantum chemical calculations using DALTON.[43] A detailed summary of the convergence test, molecular simulations on small model systems for AlGaAs and the choice of DFT functional, can be found in the supplementary material. Convergence of the results with respect to **k**-point sampling, kinetic energy cut-off of the plane wave basis set, and lattice relaxation was checked as well. AlAs has an experimental lattice spacing of 0.56695 nm and GaAs of 0.56614 nm, see ref. 21, thus the lattice mismatch for $Al_{0.5}Ga_{0.5}As$ is $\leq 0.1\%$. Relaxation of the structure resulted in negligible changes (<0.002 nm) in the atom positions. All results below were obtained using the PBE functional.[44] The PAW datasets have frozen [Ar], [Ne] and [Ar]$3d^{10}$ cores for Ga, Al and As respectively. On the basis of these results, we think that the obtained quadrupolar distributions are a good representation for this lattice.

Results and discussion

I. ^{75}As QCPMG analysis

The high quadrupolar moment of ^{75}As and its strategic anion position in the AlGaAs lattice makes it the most interesting nucleus to probe for information about the symmetry and ordering of the crystal lattice. As detailed in the experimental section, frequency-stepped QCPMG experiments[15–18] were used to obtain good sensitivity ^{75}As spectra with signals dispersed over 2 MHz. Fig. 2 displays the summation of the experimental QCPMG subspectra for each frequency offset for $Al_{0.297}Ga_{0.703}As$ and $Al_{0.489}Ga_{0.511}As$. The spectra show two narrow resonances separated by $\delta = 188 \pm 5$ ppm, in accordance with previous work[45] these lines are assigned to the signals of As[Ga_4] and As[Al_4] sites having a symmetric first coordination sphere. An arsenic nucleus surrounded by four aluminium or gallium nuclei, has a tetrahedrally symmetric structure and should therefore display no quadrupolar interaction. However, depending on the positions of the cations in the third and higher coordination spheres, there can still exist a (relatively small) EFG. Indeed, in the work by Degen *et al.*[21] a $C_q = 610$ kHz and $\eta > 0.97$ was determined for As[Ga_4] and $C_q = 820$ kHz, $\eta > 0.88$ for As[Al_4]. Here we show that these sites can be properly fitted to a Czjzek distribution, with $d = 5$ and average quadrupolar values of $C_q = 610$ and 820 kHz, as were obtained from ^{75}As nutation NMR experiments.[21] The average quadrupolar coupling constants for these two sites were fixed as the fit was not very sensitive to small changes in this parameter.

The wide resonances, not directly observed in the previous study, show distinct quadrupolar features of second-order central-transition powder patterns. A line shape with an asymmetry parameter η close to zero is easily identified. The high signal to noise ratio allowed visualization of the small but distinctive features extending from both sides of the spectrum of the spectrum indicating the presence of a species with a high asymmetry parameter. The broad resonances are assigned to ^{75}As resonances with an asymmetric first coordination shell. Based on a simple point charge model[46] we calculate a quadrupolar coupling constant of approximately 33 MHz for these coordinations. The asymmetry parameter is predicted to be $\eta = 1$ for the As[Al_2Ga_2] coordination and $\eta = 0$ for the As[Al_1Ga_3] and As[Al_1Ga_3] coordinations. The enormous width of the spectrum makes it difficult to determine the chemical shift of these resonances with any accuracy.

The spectra were fitted using an evolutionary algorithm[38] to deconvolute the signals into the contributions from each individual ^{75}As site as is shown in Fig. 2. The different quadrupolar subspectra used as library spectra for fitting the QCPMG spectra were calculated assuming ideal non-selective excitation in SIMPSON.[39] The fit with the lowest average cost

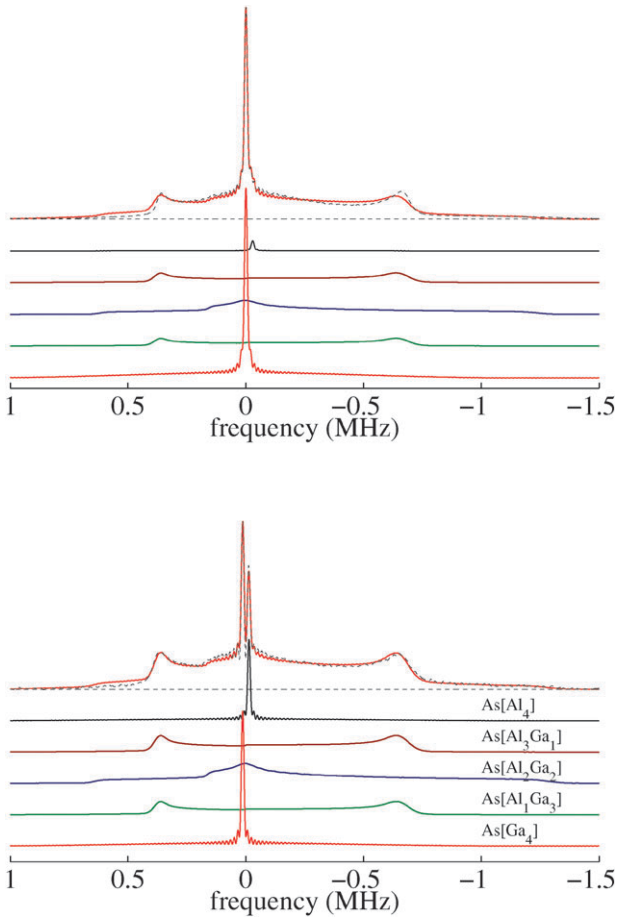

Fig. 2 (top) ^{75}As absolute sum of all 24 frequency-stepped QCPMG spectra of $Al_{0.297}Ga_{0.703}As$ (dotted line) obtained at 18.8 T and the simulated spectrum of a GA-based fit using a library of spectra simulated using the SIMPSON package (solid line). The five lower spectra show the contributions from each site. (bottom) The sum of all 22 frequency-stepped QCPMG spectra of $Al_{0.489}Ga_{0.511}As$ together with the fitted result and the individual contributions of each site. The experimental SNR was ≈120 per frequency step accumulating 5400 scans.

or χ^2 was found using the model with the least constraints, *i.e.* using a Gaussian quadrupolar distribution in the C_q and a single η value. Although good line shapes are obtained, fitting with a Gaussian distribution in C_q and η does not have a physical meaning. Therefore as has been discussed, we used the Czjzek distribution with $d = 5$ to describe the narrow resonances and extended Czjzek distributions for the broad resonances thus taking the effect of the first coordination shell on the EFG tensor into account. Based on some initial simulations and the size of the quadrupolar coupling constant of the As sites with a symmetric first coordination shell, the contribution of the higher coordination spheres was fixed to 715 kHz in the fits of the spectra.

The frequency stepped QCPMG experiment was designed to obtain undistorted lineshapes from very broad quadrupolar resonances at limited rf-field strengths. Here we are faced with the presence of very broad sites with large quadrupolar interactions and narrow lines for the As[Ga_4] and As[Al_4] resonances experiencing only very small EFGs. Indeed the spectra show some spectral distortions around the center frequency due to truncation of the narrow lines. As the off-resonance behavior of the lines with small (<1 MHz) and large (>30 MHz) quadrupolar interactions differs, adding the off-resonance spectra somewhat affects the shape of the spectrum. The broad resonances of the As[Al_1Ga_3], As[Al_1Ga_3] and As[Al_2Ga_2] coordinations could be fitted very well however, and gave consistent results in fitting the spectra of both the $Al_{0.297}Ga_{0.703}As$ and $Al_{0.489}Ga_{0.511}As$ sample. The fit parameters are summarized in Table 3.

The effective excitation differs significantly for the various sites at different resonance offsets.[12,13] Therefore we question the possibility to reliably quantify the relative intensities of the arsenic sites considering spectra obtained at different resonance offsets were added. Moreover, it is too time consuming to calculate the entire signal response, consisting of the 242 echoes, for each of the ~2000 C_q and η values, which are needed for the fitting library, using actual excitation parameters. To get a reasonable estimate for the molar ratios of the different arsenic coordinations, the on-resonance QCPMG spectra (*i.e.* with the excitation frequency in between the narrow lines) were fitted for each sample. In this case the broadened line shapes were mimicked by using the average quadrupolar coupling constant and adding a large Gaussian broadening of 50 kHz. The intensities obtained in this fit were scaled by the relative intensities obtained in a SIMPSON simulation of a single echo for each site using the actual rf field strengths as used in the experiments. The results are given in Table 3. Comparing the intensities from this analysis to the relative intensities expected for random ordering of the Al and Ga nuclei deviate for both the $Al_{0.489}Ga_{0.511}As$ and the $Al_{0.297}Ga_{0.703}As$ with the discrepancies being largest for the latter sample. In both QCPMG spectra the intensities of the As[Ga_4] and As[Al_4] resonances with small quadrupolar interactions seem to be substantially underestimated.

II. ^{75}As Hahn-echo analysis

Although the QCPMG experiments give good signal to noise ratios for the very wide ^{75}As resonances, revealing even broad low intensity features at the edge of the lines, the quantification of the relative intensities in the spectra is considered to be compromised. Therefore we attempted Hahn-echo experiments at an elevated rf-field strength to get easier processing and calibration of the spectra. The experimental results, together with unrestrained fits of these spectra are shown in Fig. 3 and 4 for $Al_{0.297}Ga_{0.703}As$ and $Al_{0.489}Ga_{0.511}As$. Indeed the signal to noise of the $x \approx 0.489$ Hahn-echo was a factor 46 lower than a corresponding QCPMG spectrum, but the main spectral features are similar to those observed in the QCPMG spectra.

The library files used for the GA analysis were obtained from SIMPSON simulations of the Hahn echo using the parameters as used in the experiments. As before, the As[Ga_4] site was fitted with a fixed Czjzek distribution with $\langle C_q \rangle = 610$ kHz and $d = 5$, the As[Al_4] site with $\langle C_q \rangle = 820$ kHz and $d = 5$, and as fixed input for the distribution of the extended Czjzek distributions for the As[Al_nGa_{1-n}], $n = 1,2,3$ sites we used the average quadrupolar

Table 3 NMR parameters obtained from fitting the experimental spectra. The reported confidence intervals are standard deviations from 7 fits. The relative intensity of each site is normalized to the echo maximum in the time domain. In the restrained fit, the S_{CuAu} order parameter was left free to fit and converged to $S = 0.01 \pm 0.01$ and $x = 0.483 \pm 0.004$. The ^{75}As quadrupolar coupling constant was calculated from the EFG by multiplication with a factor of 0.75925 MHz per 10^{20} V m^{-2}. An increased χ^2 corresponds to a poorer fit.

	Relative intensity $x \approx 0.297$				Relative intensity $x \approx 0.489$				
Site	Hahn-echo	Summed QCPMG	On-res. QCPMG	S = 0[a]	Hahn-echo	Hahn-echo S—fit[b]	Summed QCPMG	On-res. QCPMG	S = 0[a]
As[Ga$_4$]	0.14 ± 0.01		0.047	0.24	0.089 ± 0.01	0.071		0.028	0.071
As[Al$_1$Ga$_3$]	0.46 ± 0.03		0.64	0.48	0.43 ± 0.01	0.50		0.54	0.50
As[Al$_3$Ga$_1$]									
As[Al$_2$Ga$_2$]	0.39 ± 0.02		0.31	0.26	0.42 ± 0.01	0.37		0.41	0.37
As[Al$_4$]	0.004 ± 0.001		0.003	0.008	0.065 ± 0.01	0.054		0.020	0.057
	Quadrupolar coupling constant (MHz)				Quadrupolar coupling constant (MHz)				
As[Al$_1$Ga$_3$]	33.2 ± 0.1	33.2 ± 0.1	33.4		33.3 ± 0.1	33.3 ± 0.1	33.3 ± 0.1	33.4	
As[Al$_3$Ga$_1$]									
As[Al$_2$Ga$_2$]	30.3 ± 0.1	31.9 ± 0.1	33.4		30.5 ± 0.1	31.2 ± 0.2	32.5 ± 0.1	33.4	
Additional fitting parameters									
χ^2	0.57	0.74			0.98	2.14		1.02	
Fitted line broadening (kHz)	5.0	11.8	2.0		12.4	12.4	8.0	4.0	

[a] Theoretical Intensities corresponding to $S_{CuAu} = 0$ (eq. 6) [b] Fit of the Hahn-echo data imposing the CuAu order parameter model.

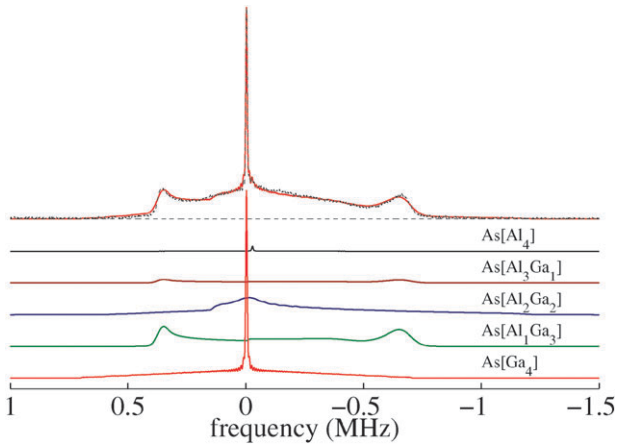

Fig. 3 The experimental ^{75}As Hahn-echo of $Al_{0.297}Ga_{0.703}As$ (dotted line) obtained at 18.8 T together with the fitted spectrum (solid line) using a genetic algorithm (see text). The five lower spectra show the individual contributions from each arsenic site. Spectra were averaged for 166 000 scans leading to an SNR ~ 80.

coupling constant of the two symmetric sites $\langle C_q \rangle = 715$ kHz, the EFG principal values $V^{\eta 0}$ and $V^{\eta 1}$ from the first coordination shell of these sites were left free to fit. As is clear from the fits of the $x \approx 0.297$ (Fig. 3) and 0.489 samples (Fig. 4), the spectral deconvolution using the Czjzek and extended Czjzek distributions works very well for all spectra. The quadrupolar interaction parameters obtained from these Hahn-echo data are in good agreement with those obtained from the QCPMG data. The quadrupolar coupling constant for the As[Al$_2$Ga$_2$] site is slightly lower which is attributed to the less efficient excitation of the broad features at the edges of the Hahn-echo spectra. The relative intensities obtained from the these spectra differ significantly from those estimated from the on-resonance QCPMG spectra. The intensities of the narrow lines seem much more realistic now, but the values obtained from the simulations still differ from those expected for an order parameter model.

As an alternative we imposed the CuAu order parameter model in the fitting procedure of the $x \approx 0.489$ spectrum, leaving the S_{CuAu} free to fit and the composition value x free to vary within 2%, which will constrain the five relative intensities. The latter was implemented to allow for experimental errors in the composition x, from the growth process. Fig. 4 shows the fit of the $Al_{0.489}Ga_{0.511}As$ spectrum. The best fit was obtained for $S = 0.01$ and $x = 0.483$. Compared to the free fit with $\chi^2 = 0.98$ the χ^2 increased to 2.14, see Table 3. The restrained fit imposes the relative intensities defined by the long-range order parameter and it was observed that the least square deviation increased. Nevertheless, this restrained fit is considered reasonable, since the spectra show no indication of long range order in the samples in accordance with X-ray data. Using the same approach the $Al_{0.297}Ga_{0.703}As$ sample shows a very different picture, however. In this case it proved impossible to fit the relative intensities complying to an order parameter model.

To estimate the reproducibility of the fit procedure, synthetic spectra were generated with random noise of the same order of magnitude and with the same bandwidth as was visible in the experimental spectrum. The standard deviation of the relative intensities due to white noise, did not exceed 2%. The confidence intervals for the relative intensities were determined from the standard deviation of seven different fits, 1% error margin was added to each site to account for systematic errors. The confidence intervals are smaller for the $x \sim 0.489$ sample, caused by the more distinctive shape of the spectrum. p_1 and p_3 were undistinguishable and considered as one intensity $p_1 + p_3$.

The spectra of both the $Al_{0.489}Ga_{0.511}As$ and the $Al_{0.297}Ga_{0.703}As$ sample do not show distinct signs of long-range order. The distributions in quadrupolar interaction parameters clearly indicate positional disorder in the occupance of the Al and Ga sites in the higher coordination spheres of all the arsenic in the lattice. Remarkably, however, the relative intensities of these sites do not comply with an $S = 0$ situation using the order parameter model as used for the description of

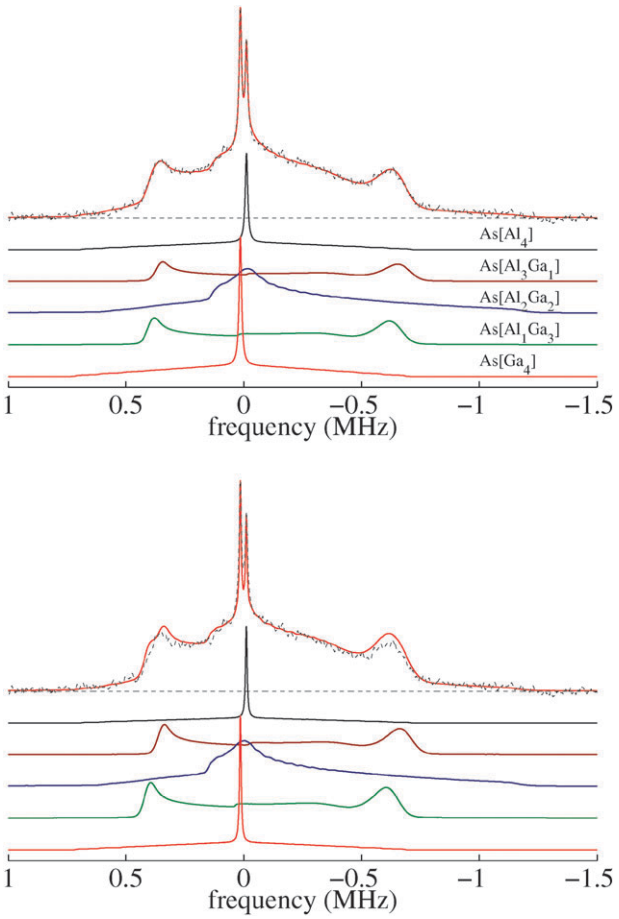

Fig. 4 (top) The experimental ^{75}As Hahn-echo spectrum (18.8 T, 166 000 scans, SNR $\sim$ 80) of $Al_xGa_{1-x}As$, $x = 0.489$ (dotted line) together with the fit (solid line). The five lower spectra show the contributions from each site. (bottom) Restrained fit imposing a CuAu order parameter model, where the S-parameter was left free to vary and the x could vary within 2%. The relative intensities fitted to $S = 0.01$ and $x = 0.483$. The five lower spectra show the contribution from the individual sites.

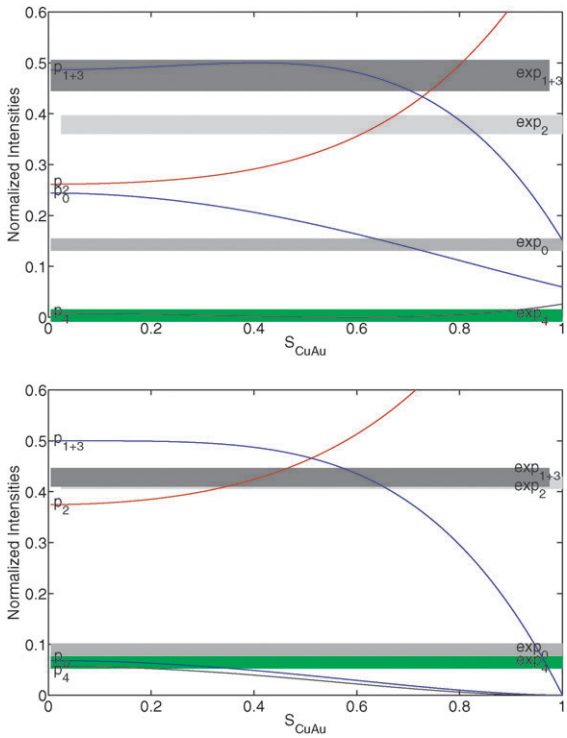

Fig. 5 (top) The theoretical relative intensities p_n as a function of the CuAu order parameter S for $x = 0.297$, see eqn (6) (solid lines). The experimental relative intensities $\exp_n$ of the Hahn-echo are plotted as vertical bars representing their confidence intervals + 1% systematic model error per site. (bottom) $x = 0.489$.

XRD data. Although a restrained fit of the $x \approx 0.489$ sample did fit to $S = 0$. For this sample the results show a similar observation as that by Tycko *et al.*,[22] *i.e.* that the relative NMR intensities of different C atom coordinations in $A_xB_{1-x}C$ type materials can be used to set an upper limit to the long range order parameter in such materials. The fitted relative intensities for the $x \approx 0.297$ sample deviate strongly from the order parameter model and could not be fitted to any S (Fig. 5). It should be noted that, the order parameter model as used here, only considers the average long range order and does not take any specific short range order into account. Therefore, it is worthwhile to explore further if the NMR spectra contain any information about local order on a nm scale. Short range ordering contains similar surroundings/sites $As[Al_nGa_{4-n}]$ $n = 0$–4, but for $n = 1,2,3$ each surrounding has a discrete set of tensor orientations (see Section DFT).

III. ^{69}Ga nutation and 3QMAS

To independently verify the random distribution of Al and Ga over the lattice, a series of static nutation experiments were performed for ^{71}Ga and ^{69}Ga at 14.1 T for the $x \sim 0.297$ sample. Here we focus on the ^{69}Ga results because of its larger quadrupolar moment, giving the largest sensitivity to electric field gradients. In the case of an ordered structure, or domains with high ordering, there should be a Ga resonance without any quadrupolar broadening in the spectrum. In ^{69}Ga static spectrum only one (Gaussian) signal is present at $\sim$6 ppm with respect to GaAs. In a nutation experiment the line shape is dependent on the ratio of the quadrupolar frequency ν_Q and the rf-field strength ν_1. The nutation spectra in Fig. 6 show rather featureless lines, as was also observed earlier for $x \sim 0.489$ by Degen *et al.*[21] This is attributed to the effect of a distribution in quadrupolar parameters and to some extent the effect of RF inhomogeneity. Degen *et al.* found a $C_q = 520$ kHz and $\eta > 0.97$ for $x \approx 0.489$. We fitted the data using Czjzek distributions with d ranging from 1 to 5 and for $\sigma = 100$ to 600 kHz. It is verified that the simulated nutation spectra for $\eta \sim 1$ (dashed thin line), or a Czjzek distribution (solid line) do not differ much. Although it was not possible to uniquely fit the nutation data to a specific model, the spectra clearly preclude the existence of a Ga site with a near zero quadrupolar interaction or/and low η. This rules out the presence of highly ordered domains in this sample.

An additional verification of the absence of well-defined Ga sites in ordered structures comes from ^{69}Ga static, MAS and 3QMAS spectra. The ^{69}Ga line width contains different contributions including quadrupolar and dipolar broadening and broadening due to the exchange interaction.[47] At 9.4 T the

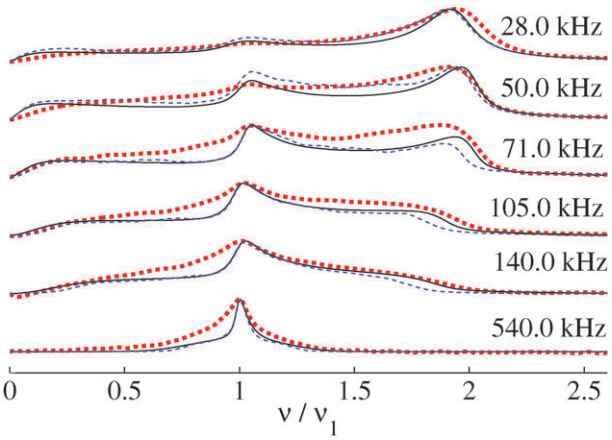

Fig. 6 Experimental ^{69}Ga static nutation spectra obtained at 14.1 T using different rf field strengths for $Al_{0.297}Ga_{0.703}As$ (dashed thick lines). The solid lines represent SIMPSON simulations of the nutation spectra assuming a Czjzek[25] distribution in the quadrupolar interaction parameters. Shown is the best fit using $d = 5$, $\langle C_q \rangle = 2{\cdot}\sigma = 0.60$ MHz. The dashed thin lines were calculated using $\eta = 1$ and $C_q = 0.80$ MHz.

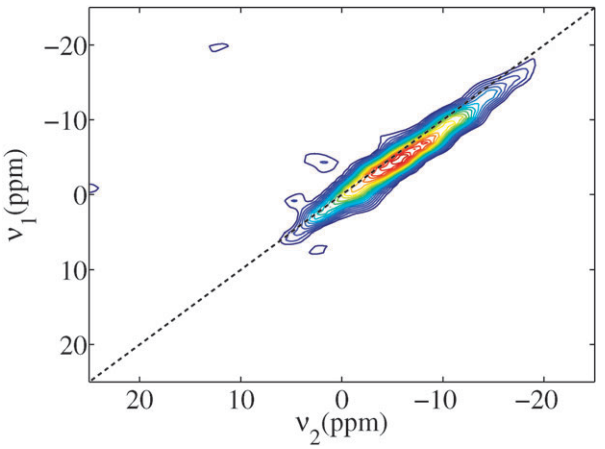

Fig. 7 Sheared ^{69}Ga 3QMAS spectrum obtained at 14.1 T. A z-filtered 3QMAS spectrum was acquired using rf-field strenghts of 120 kHz and 20 kHz for the hard (5.4 respectively 1.8 μs) and selective (6 μs) pulses, respectively. The ν_1 dimension was scaled by 9/34 to get an easy interpretable ppm scale. In this convention a hypothetical resonance without quadrupolar interaction has the same shift value in ppm on both axes.

static Gaussian full width at half maximum (FWHM) is 2.8 kHz, using 15 kHz Magic Angle Spinning (MAS), the shape remains Gaussian with a FWHM of ~1.6 kHz. The second order quadrupolar contribution to the linewidth is of the order of $(3/64){\cdot}(C_q^2/\nu_z)$.[48] With quadrupolar coupling constants up to ~800 kHz this contribution is less than ~300 Hz. Therefore the main contributions to the linewidth originates from a distribution in isotropic chemical shift and/or exchange interaction. This is also clear from the ^{69}Ga (3Q)MAS spectrum obtained at 14.1 T for $Al_{0.297}Ga_{0.703}As$ shown in Fig. 7. The broadening of the spectrum mainly extends along the shift axis. From the position of the center of gravity in both directions, $\delta_1 = -5.1$ ppm and $\delta_2 = -7.4$ ppm, an average isotropic chemical shift $\delta_{iso} = -6.0$ ppm and an average quadrupolar induced shift $\delta_{qis} = -1.45$ ppm was determined resulting a quadrupolar product $P_Q = C_Q \cdot \sqrt{1+\eta^2/3}$ of 730 kHz in accordance with the nutation data. Again there is no indication of a site with a well-defined (small) quadrupolar coupling constant and asymmetry parameter which would be expected for sites in ordered domains in the sample.

DFT Modeling

To gain more insight in how structural variations translate into NMR parameters, in particular the quadrupolar interaction and its distributions, we need to simulate many different structures and relate these structures to the NMR parameters. It has been shown that a point charge model is not able to properly predict the EFG distributions in these type of systems.[49] A good model should rely on first-principles input data. We address the problem in two ways: first, we make ordered and randomized structural models using supercells, with the compositions $x = 0.5$ and $x = 0.3125$ and calculate their EFGs with DFT. This approach also allows one to access the energetics of these models. Because of the computational cost the number of configurations studied and hence the statistical quality of the EFG distributions is limited. Moreover, only a few values of the order parameter S can be realized. This "supercell model" approach provides a semi-quantitative understanding. In the second approach, called the "multipole model", we exploit the additivity of EFGs in AlGaAs. This allows for calculating large numbers of structures, high quality statistics and many values of S to be studied. In this part we restrict ourselves to a computation with equal amounts of Al and Ga present. Finally, we will show that the obtained distributions for $S = 0$ concur with the analytical result of the extended GIM, described by Le Caër and Brand.[26]

I. Supercell models

To approximate the distributions observed in the experimental spectra of the $x \approx 0.489$ sample by theory, twelve structures with $x = 0.5$ were simulated. Cubic-shape supercells were used, containing 16 formula units in a $2 \times 2 \times 2$ arrangement of conventional zinc blende unit cells, *i.e.*, $Al_{16}Ga_{16}As_{32}$. Here we discuss the change in orientation of the tensors, as the occupation of the cation lattice goes from full CuAu ordering to a more random arrangement. One structure was created with full CuAu ordering ($S_{CuAu} = 1$) and one with partial high ordering, $S_{CuAu} = 0.875$. Ten structural models were created using random positioning of the Al and Ga cations, all with $S_{CuAu} \leq 0.25$. The calculated principal z-axis of the EFG tensor is plotted for each atom in Fig. 8. All atoms were kept at their ideal lattice positions.

Full order. In a fully ordered CuAu $Al_{0.5}Ga_{0.5}As$ lattice, the only ^{75}As site present is As[Al_2Ga_2]. The principal z-axis of the EFG tensor of this site always lies in the As $x - y$ plane (under an angle of 45 degrees). The in-plane orientation changes by 180° between adjacent As layers.

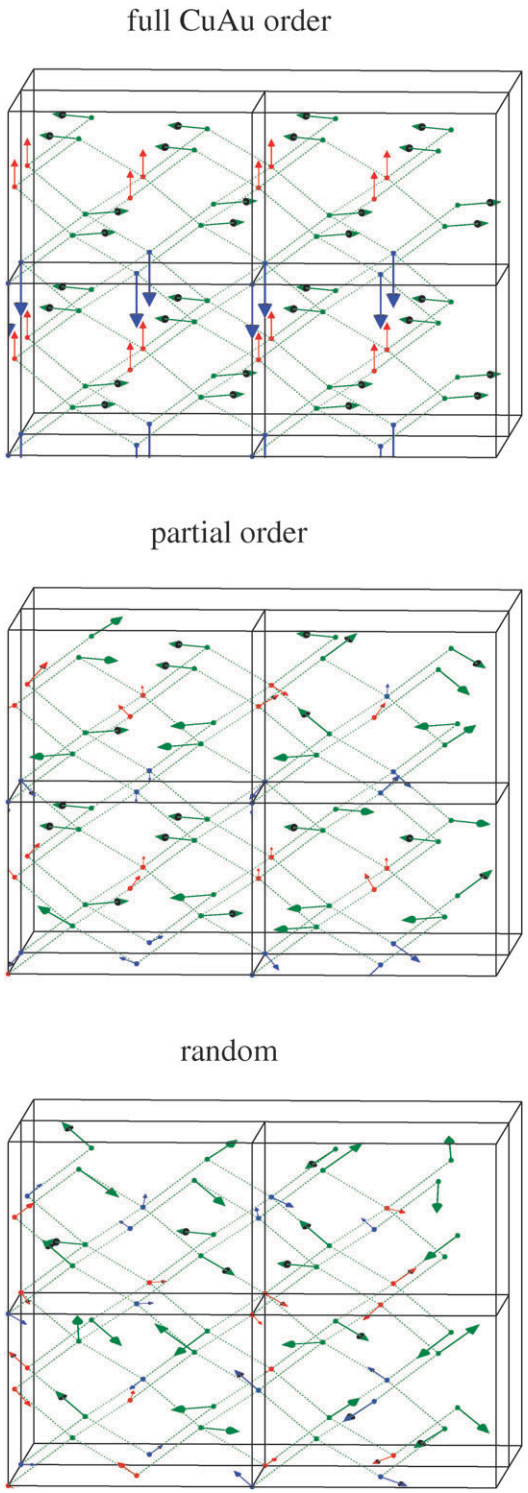

Fig. 8 $2 \times 2 \times 2$ (conventional unit) cells of a $Al_{0.5}Ga_{0.5}As$ lattice containing 64 atoms. The horizontal layers from bottom to top are Al (blue), As (green), Ga (red), As, Al, As, Ga, As. The arrows display the direction of the V_{zz} principal EFG tensor direction for each atom. (top) fully ordered lattice with $S_{CuAu} = 1$, (middle) partially ordered lattice with $S_{CuAu} = 0.875$, (bottom) randomly ordered lattice with $S_{CuAu} \leq 0.25$.

Partial order. Swapping only two cations in a 2×2 cell results in a partially disordered but still highly ordered structure, with a small distribution in the principal EFG z-axis direction for the $n = 1,2,3$ sites and a spread of $\Delta\eta = \pm 0.03$. 8 of the 32 As atoms are $n = 1,3$ sites. As depicted in the figure, the Principal Axis System (PAS) of the $As[Al_1Ga_3]$ ($n = 1$) or $As[Al_3Ga_1]$ ($n = 3$) EFG tensors have their z-axis oriented along any body diagonal of a cube, *i.e.* in one of 4 possible directions. The main difference between $As[Al_3Ga_1]$ and $As[Al_1Ga_3]$ is the positive/negative sign of the quadrupolar coupling. The principal z-axis of an $As[Al_2Ga_2]$, $n = 2$ EFG tensor has 6 possible orientations along all *face* diagonals of a cube.

Random. In a random lattice the three sites with $n = 1,2,3$ occur with different relative intensities and the EFG distribution within all sites is much stronger. Ten different random models were used to estimate the distributions in the tensor values. In Fig. 9 we approximate the distributions for the $n = 1$ and $n = 3$ sites with a Gaussian-type distribution as used by Jäger and coworkers.[23] Although the simulated EFG data roughly follow that of a Gaussian distribution, the statistics do not allow a definite conclusion on the shape of the distribution, *i.e.* we cannot decide whether it is a Gaussian. Indeed, on physical grounds we do not expect a Gaussian distribution. Evidently we need a model that allows for higher quality statistics (see next section). $As[Al_4]$ and $As[Ga_4]$ sites are even more rare in the generated structures, so we do not attempt to fit their distributions with any functional form.

The averages and standard deviations of the V_{zz} and η distributions for $x = 0.5$ are listed in Table 5. Similar calculations were carried out for the composition with $x = 0.3125$ as summarized in Table 6. Inspecting the tables, we see that for both compositions the agreement of the average ^{75}As V_{zz} and η with the experimental results is reasonable for the random models, for all $n = 0$–4. For the $\langle V_{zz} \rangle$ of the $n = 0$ and $n = 4$ sites the relative difference between calculation and experiment is larger, with calculations overestimating the average EFGs. We have to keep in mind that these EFGs are very small, since they are caused by distant coordination shells. The neglect of the contributions of the arsenic core states might explain this discrepancy (see supplementary

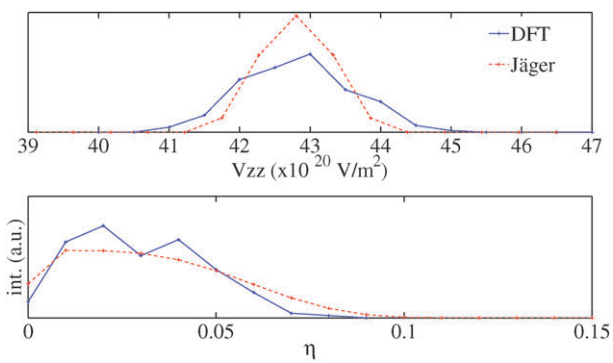

Fig. 9 V_{zz} and η distributions for $As[Al_1Ga_3]$ and $As[Al_3Ga_1]$ sites. Solid line: DFT calculations for 10 random supercells of the $Al_{0.5}Ga_{0.5}As$ lattice. The dotted line shows a Jäger type[23] Gaussian distribution with $\langle C_q \rangle = 33.0$ MHz, a HWHM = 0.4 MHz and $\eta = 0.03$.

Table 4 Total energy of the $Al_xGa_{1-x}As$ supercells, depending on the composition and order parameter. The partially ordered structure for $x = 0.5$ is displayed in Fig. 8. "Random 1–10" denotes 10 different near random structures with low order parameter S. For $Al_{10}Ga_{22}As_{32}$ with $x = 0.3125$ "order 1" has a relatively high ordering, with full Ga occupation of one layer and 2 identical cations in the farthest layer. "order 2" has full Ga occupation of one layer and 2 identical cations in the nearby layer. "order 3" has 5 identical cations in layers 1 and 2 (small cluster)

	Total energy (eV/cell)	S_{CuAu}
$Al_{16}Ga_{16}As_{32}$		
Fully ordered CuAu	−283.098	1
Partially ordered	−283.100	0.875
Random 1–10	−283.123 – −283.150	0 – 0.25
$Al_{10}Ga_{22}As_{32}$		
Order 1	−277.186	0.5
Order 2	−277.214	0.375
Order 3	−277.163	0
Random 1–10	−277.163 – −227.188	0 – 0.375

information). For ^{69}Ga the agreement for $x = 0.5$ also seems good, at least as far as the average V_{zz} is concerned. The average ^{27}Al V_{zz} is considerably underestimated in these calculations, however. This is probably also related to the neglect of core contributions (see supplementary information).

Table 4 (upper part) summarizes the calculated total energies for the ($x = 0.5$) structures displayed in Fig. 8. The random structures all have lower total energy than the fully and partially ordered structures. The energy differences are small: $\Delta E \approx 0.04$ eV/64 atoms = 0.6 meV/atom. So we do not observe a significant thermodynamic driving force for ordering.

For the $x = 0.3125$ composition perfect CuAu ordering is not possible. Therefore, we compare the random structures with several ordered models with $S \neq 1$. One of the ordered models has the lowest total energy, but the differences in energy with other structures are very small. Keeping in mind that there is also an entropic contribution favoring disorder, we again cannot conclude that there is a tendency towards ordering.

II. Multipole model

As good statistics requires a large number of configurations, we need a very fast method to calculate the EFGs for each new configuration. Below we first describe this method, provide a physical justification, give details on generation of the configurations and analyze the results. This model reproduces the absolute EFG tensor values with an accuracy of ~10%, compared to an independent direct DFT calculation.

We start with a single DFT calculation on a large cubic super cell consisting of $4 \times 4 \times 4$ conventional zincblende unit cells. All cations are Ga, except for one, *i.e.*, the cell has composition $AlGa_{255}As_{256}$. The DFT calculation yields the EFG tensors for all 256 As atoms so that we know the As EFG as a function of $\mathbf{r}_{AsGa}$, the vector from Ga to As. For any possible configuration of any possible cell with composition $Al_nGa_{(256-n)}As_{256}$ we calculate the EFGs by multiple addition: For each Ga we add its contribution to the As EFGs at displacements $\mathbf{r}_{AsGa}$ using the result of the single DFT calculation. Once the contributions due to all Ga's have been added, the As V_{zz} and η are obtained by diagonalization. This procedure is very fast, as it obviates the need for a separate DFT calculation for each different atomic configuration. It can be somewhat refined at negligible computational cost. The distributions $P(|V_{zz}|,\eta)$ are modeled as a function of the order parameter S_{CuAu}. On the computer we generate many, 3×10^6, configurations by randomly placing cations in the $4 \times 4 \times 4$ unit cell. For each configuration we determine the order parameter S_{CuAu} from the definition in eqn (1) and then V_{zz} and η for all atoms. Counting the number of occurrences of the (V_{zz},η) values then yields the quadrupolar distributions as displayed in Fig. 11.

Now let us consider the assumptions that go into this procedure. Suppose we interchange one Al for a Ga atom in $Al_xGa_{1-x}As$. In first order only the polar bonds between the Al/Ga and its 4 neighboring As are affected. The charge redistribution preserves the local tetrahedral symmetry, hence the leading order induced charge moment will be that of an octopole. These octopole (and higher) terms will give rise to an electric field at nearby As sites. The field, in turn, will be screened by the other atoms on the $Al_xGa_{1-x}As$ lattice. This screening is described by the microscopic dielectric function $\varepsilon(\mathbf{r},\mathbf{r}')$. In our approach, we implicitly assume this function is independent of the local chemical composition (indeed this is our central assumption). This is reasonable as the (macroscopic) dielectric constants of AlAs and GaAs do not differ much ($\varepsilon_\infty = 8.2$ respectively $\varepsilon_\infty = 10.8$).[50] We have also checked this assumption by recalculating the EFGs with DFT for a limited number of random configurations (in smaller super cells). Note that we also neglect the effect of local atomic relaxations. This is justified as the lattice match between AlAs and GaAs is nearly perfect and structural relaxations are very small.

In Fig. 10 the arsenic V_{zz} as obtained by DFT in the $AlGa_{255}As_{256}$ and $Al_{255}GaAs_{256}$ super cells is plotted as a function of the distance to respectively the Al or Ga atom. Note that only beyond the third As shell the contributions to the V_{zz} become very small. This occurs at a distance well below half of the size of the super cell (2.25 nm/2). So our super cell is chosen sufficiently large that spurious contributions from periodic images are avoided.

Remarking that the screening is dominated by the atoms in the first shell, we can improve our modeling of the As[Al_4] sites. Based on a DFT calculation with a single Ga ($Al_{255}GaAs_{256}$, called "Ga in a sea of Al") we correctly describe the screening by the first shell, whereas with the calculation based on $AlGa_{255}As_{256}$ ("Al in a sea of Ga") all first shell atoms are Ga. The latter would be more appropriate for the As[Ga_4] sites. More information on the difference between the "Ga in a sea of Al" and "Al in a sea of Ga" results can be found in the supplementary information.

As each configuration of $Al_{128}Ga_{128}As_{256}$ yields a specific EFG and η, an EFG distribution can be constructed relatively fast from many occurrences with similar order parameters S_{CuAu}. Configurations that do not match the "stoichiometry" constraint $Al_{128}Ga_{128}As_{256}$ are discarded. The configurations are sorted by S_{CuAu} that is calculated using eqn (1).

Fig. 11 shows the variation in the As[Al_nGa_{4-n}] EFG distributions, as calculated with the "multipole model" for different CuAu order parameters S_{CuAu}. As S becomes larger,

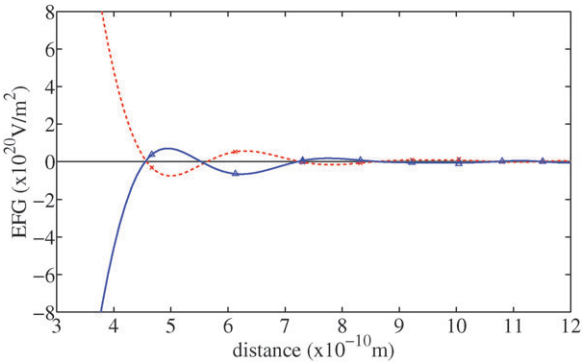

Fig. 10 Principal EFG component V_{zz} for ^{75}As as a function of the distance to a Ga or Al atom in the AlGaAs lattice. The data were calculated using a $Al_{255}GaAs_{256}$ super cell, referred to as "Ga in a sea of Al" (dotted line) or a $AlGa_{255}As_{256}$ (solid line) super cell, "Al in a sea of Ga". In the first shell V_{zz} (not shown) attains values of $\pm 43.6 \times 10^{20}$ V m^{-2}. The curves are a guide to the eye.

in general, the average As V_{zz} and η values increase. In the lower S range, the distributions are rather insensitive to S (compare the $S = 0$ and $S = 0.5$ curves). Increasing S to 0.5, all As V_{zz} distributions become more symmetric, except for As[Al_2Ga_2] which develops a pronounced asymmetry. For higher S, a pattern with shoulders and "spikes" develops. A similar observation was described analytically in the work of Le Caër *et al.*[26] (their Fig. 4 and 5). The quadrupolar distributions for the $n = 0$,4 sites can be described with Czjzek distributions for $d = 5$ and $S = 0$. V_{zz} of the $n = 1$–3 sites are dominated by the atoms in the first coordination shell of the arsenic and the average V_{zz} typically changes by ~3% going from $S = 0$ to $S = 1$ and the distribution narrows.

As expected, the $n = 0$ and $n = 4$ As site provide a much more sensitive probe to the degree of disorder, and a concomitantly weaker EFG (Fig. 12). The degree of (dis)order has an even more dramatic impact on the Ga distributions: not only does the average V_{zz} increase from $\sim 1.0 \times 10^{20}$ V m^{-2} for $S = 0$ to $\sim 1.8 \times 10^{20}$ V m^{-2} for $S_{CuAu} = 1$ (an 80% increase) but also the width of the distribution is reduced by almost an order of magnitude. The wild oscillations in these η patterns might be attributed to an insufficient number of configurations, as the number of configurations decreases with increasing S.

III. The extended GIM model

We will now focus on the simulations for $S = 0$. As shown in the upper figure of Fig. 13, for a lattice with random order, the distribution in the quadrupolar parameters of As[Ga_4] and As[Al_4] derived from the "multipole model" perfectly match a Czjzek distribution with $d = 5$ and an average quadrupolar constant σ. Such distributions are isotropic and rotation invariant. The quadrupolar distributions obtained for the $n = 1,2,3$ sites for the $S = 0$ structures could be matched when a defined first shell tensor was added the distributions in EFG due to the disorder in the higher coordination sphere as described earlier. In fact, these distributions also matched the analytical extended GIM as described by Le Caër and Brand.[26] The $n = 1$ and $n = 3$ distributions have $\eta(0) = 0$ and match with their eqn 61, see bottom figure of Fig. 13. The $n = 2$, *i.e.*, $\eta(0) = 1$ fit in Fig. 13 cannot be obtained with a simplified analytical expression, such as eqn 61 in Le Caër and Brand. This distribution was obtained numerically, by integrating eqn (10) over all three Euler angles ($0 \leq \alpha < 2\pi$, $0 \leq \beta < \pi$, $0 \leq \gamma < 2\pi$).

We also modeled the EFG distributions of the Ga and Al sites for the disordered $S = 0$ situation using the additivity model of the tensor values, applying the "Al in a sea of Ga" or "Ga in a sea of Al" approach. These distributions appeared to be more complex and do not follow the regular or extended Czjzek distribution. For Ga the overlap with a Czjzek distribution with $d = 5$ is displayed in Fig. 14. Even though the cations are randomly positioned, the calculated distribution is more structured than a Czjzek with $d = 5$. We attribute this to the fact that for gallium the distribution mainly originates from the closer, second shell. This is closer than the case of the arsenic $n = 0$ and $n = 4$ sites, where the first and second shell are isotropic. So we conclude that the effect of the closer second shell cannot be modeled with a fully random model such as the Czjzek distribution with $d = 5$.

IV. Comparing theory and experiments

The average EFG values can be predicted well using our DFT approach as implemented in the VASP package. For arsenic, we approach the experimental results quite satisfactory: For As[Al_1Ga_3], As[Al_3Ga_1] and As[Al_2Ga_2] sites the discrepancies between theory and experiment for *e.g.*, $\langle V_{zz} \rangle$ ($\langle C_q \rangle$) are substantially below 10% for both sample compositions $x = 0.5$ and $x = 0.3125$. For the As[Al_4] and As[Ga_4] sites, the discrepancies are somewhat larger. It should be noted, however, that these EFGs are two orders of magnitude smaller. The differences could be due to small errors arising from the neglect of the response of (deep) core electrons. The limited number of random supercell models that could be generated do not allow to make predictions about the exact shape of the distributions $P(V_{zz},\eta)$, however. For $x = 0.5$ we showed that the combined EFG distribution of the As[Al_1Ga_3]/As[Al_3Ga_1] sites (Fig. 9) still had insufficient statistical quality. This distribution was derived from an average of 176 + 113 = 309 different As sites, see Table 5. For the As[Ga_4] and As[Al_4] sites we can only average 17 and 14 configurations respectively, so it is really impossible make any statement on the shape of the distribution function $P(V_{zz},\eta)$ based on this data.

The multipole model with $x = 0.5$ was based on 3×10^6 configurations, where each configuration was constructed out of 256 As atoms. This allows for reliable statistics, also for the relatively rare As[Al_4] and As[Ga_4] sites. The additional approximations result in some errors, but all ($n = 0$–4)V_{zz} averages are well within the expected ~10% of the supercell models. The data obtained from the As[Al_4] site seems to deviate more, but note that the estimated RMS error in the average, obtained with the supercell models, is $0.33 \text{ MHz}/\sqrt{14} = 0.09 \text{ MHz} \sim 8\%$. With the multipole model, the discrepancy between theory and experiment for As[Al_4] is reduced to ~15%. The As[Ga_4] has, unfortunately, increased a bit to ~25%. As these EFGs are very weak, we think these results are very reasonable.

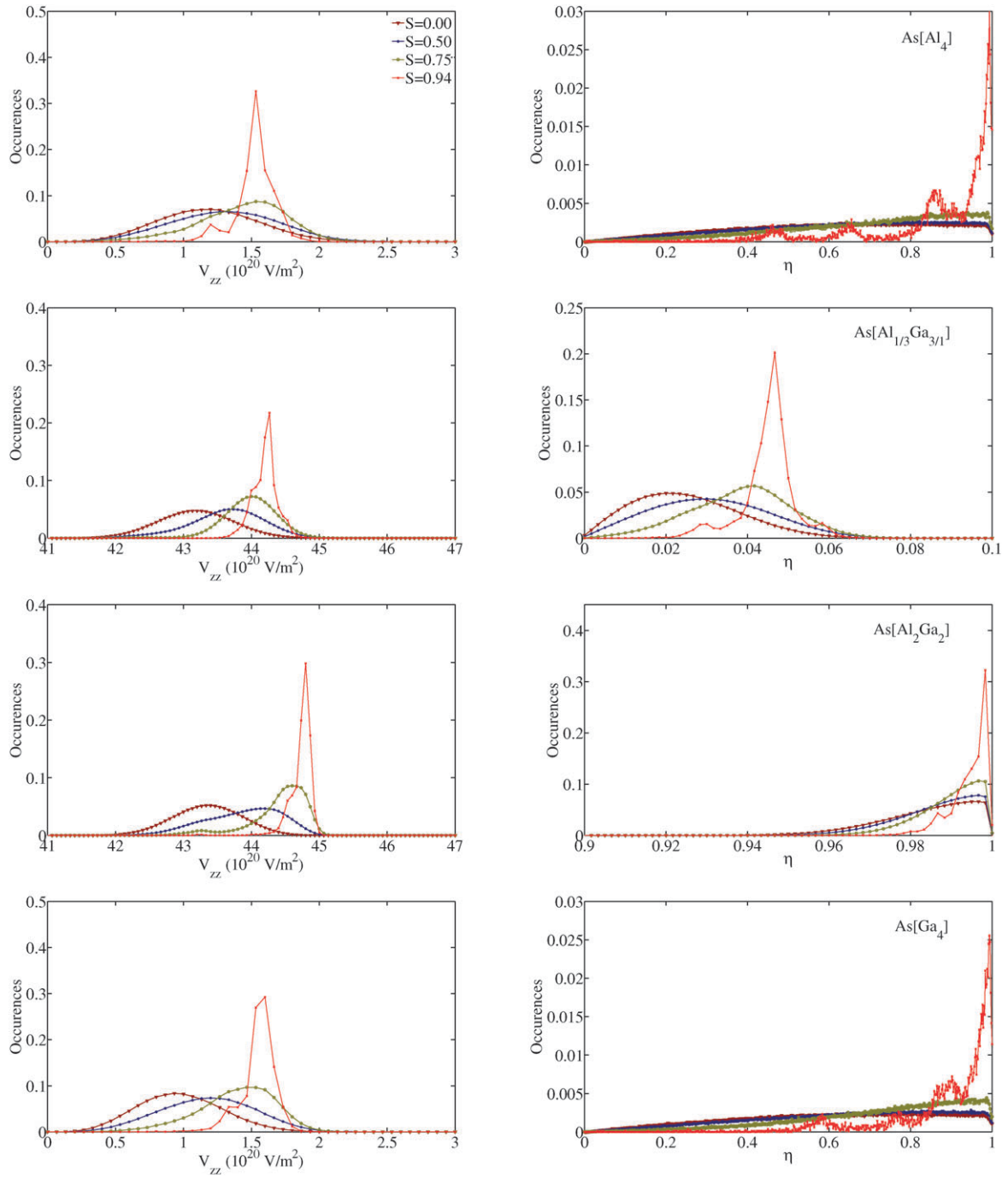

Fig. 11 V_{zz} (left) and η (right) distributions of the different arsenic sites in $Al_{0.5}Ga_{0.5}As$ for different order parameters S_{CuAu} = 0,0.5,0.75,0.94 as obtained from DFT-based modeling of a $Al_{128}Ga_{128}As_{256}$ super cell. The distribution in the quadrupolar parameters for the As[Al$_4$] site was simulated using the "Ga in a sea of Al" model, all other sites were calculated using the "Al in a sea of Ga" approach.

The main advantage of the multipole model is that we can now study the distribution functions themselves, even for the difficult sites As[Al$_4$] and As[Ga$_4$]. We found (Fig. 13) that the latter are accurately described by Czjzek distributions with d = 5. Thus we provide a first-principles basis to support this model. Using these results to describe the "amorphous" background, we then find that the EFG distributions of the As[Al$_1$Ga$_3$], As[Al$_3$Ga$_1$] and As[Al$_2$Ga$_2$] sites are all accurately described by the extended Czjzek distribution.

Conclusions

A judicial choice of rf-coil diameter makes it possible to observe ^{75}As spectra from thin film material of AlGaAs grown by MOCVD. Reducing the coil diameter provides the sensitivity to study the limited amount of material available from a single film. Additionally the small diameter of the coil enables the generation of rf-fields large enough to efficiently excite the entire bandwidth of the arsenic spectrum. Frequency-stepped QCPMG spectra and single Hahn-echo experiments

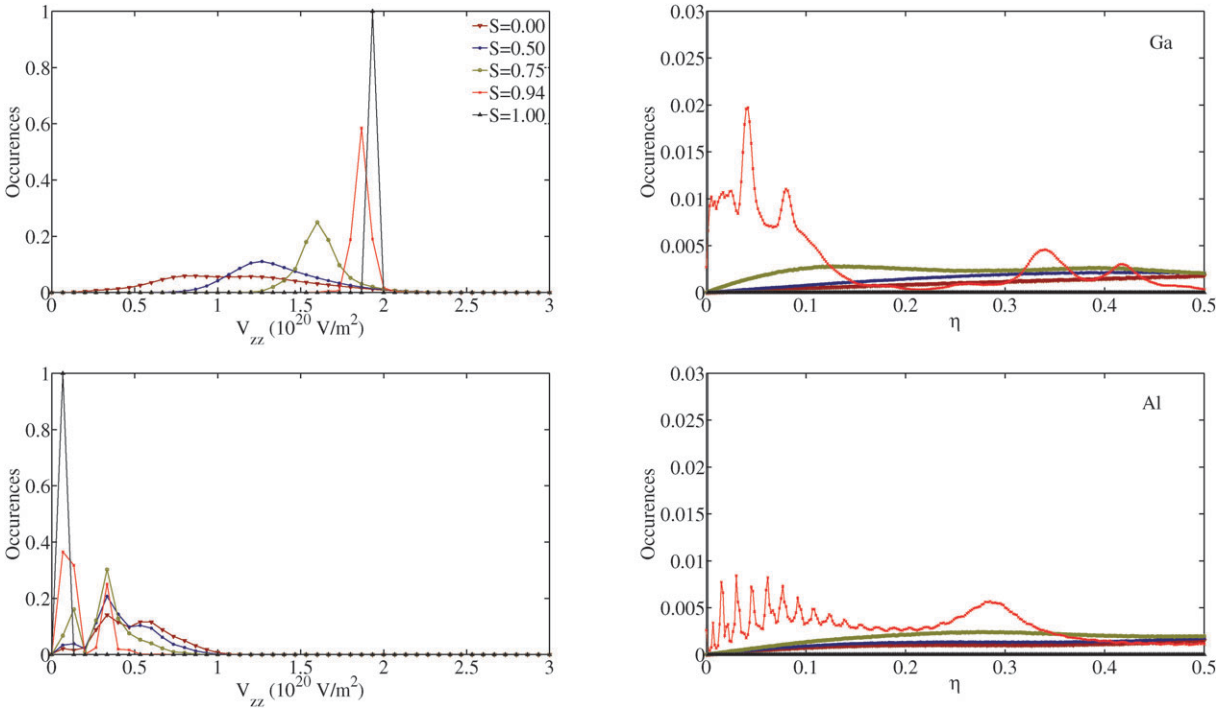

Fig. 12 V_{zz} (left) and η (right) distributions at the Al and Ga sites in $Al_{0.5}Ga_{0.5}As$ for different order parameters S_{CuAu} = 0,0.5,0.75,0.94 and 1 as obtained from DFT-based modeling in a $Al_{128}Ga_{128}As_{256}$ super cell. For S = 1 all occurrences have η = 0. The Ga distribution was simulated using "Al in a sea of Ga". The Al distribution was simulated using the "Ga in a sea of Al" model.

both reveal the presence of five resonances assigned to $As[Al_nGa_{1-n}]$, n = 0–4 with NMR parameters mostly depending on the symmetry of the first coordination shell. The quadrupolar coupling constant varies from less than 1 MHz for the symmetric n = 0 and n = 4 coordinations, to over 30 MHz for the asymmetric n = 1,2,3 coordinations. Using an evolutionary algorithm, the spectra can be decomposed into the individual contributions from the different As resonances. The frequency-stepped QCPMG data allow the most accurate determination of the quadrupolar interaction parameters; this is of particular importance for the $As[Al_2Ga_2]$ site whose low intensity discontinuities from the η = 0 second-order quadrupolar powder pattern at the edge of the spectra are most pronounced in the QCPMG spectra. These spectra, containing resonances from sites with small and large quadrupolar interactions can not produce reliable relative intensities for the different sites, however, due to the varying excitation efficiencies for the different sites at varying resonance offsets. The quadrupolar interaction parameters extracted from the Hahn-echo experiments are in accordance with those obtained from the QCPMG data, except for the $As[Al_2Ga_2]$ site that comes out slightly smaller. As expected the Hahn-echo experiments are less sensitive compared to the QCPMG data. The advantage of the Hahn-echo data is that it is possible to determine the relative intensities of the As sites.

Imposing an order parameter model on the fits gives a satisfactory solution of S = 0 for the $Al_{0.489}Ga_{0.511}As$ sample, meaning the Al and Ga nuclei are randomly distributed over their lattice sites. For the $Al_{0.297}Ga_{0.703}As$ material no satisfactory fit using the order parameter model could be obtained. These results indicate that there is no long-range order present in both samples. The structural disorder in the occupancy of the Al/Ga sites is also reflected in the distributions of the quadrupolar interaction parameters of the As sites. The symmetric $As[Al_4]$ and $As[Ga_4]$ sites have finite quadrupolar interactions with a distribution which can be described by a Czjzek distribution with uncorrelated Gaussian distributions in the five independent electric field gradient tensor values. This reflects the random disorder in the higher coordination spheres of these Arsenic sites which is isotropic and rotation invariant. For the As sites $As[Al_nGa_{1-n}]$, n = 1,2,3 with a mixed first coordination shell, the electric field gradients can be described by a summation of the EFG of the first coordination sphere to a Czjzek distribution resulting from the disorder in the higher coordination spheres. This "background" Czjzek distribution is identical to the one obtained for the symmetric $As[Al_nGa_{1-n}]$, n = 0,4 sites.

Field dependent ^{69}Ga MAS NMR data, nutation and 3QMAS spectra of both $Al_xGa_{1-x}As$ (x = 0.489 or x = 0.297) samples did not show the presence of Ga species with a zero or very small quadrupolar interaction as would be expected in the case of formation of ordered structures supporting the conclusion of random ordering.

DFT calculations of the electric field gradient tensors based on the PAW method implemented in VASP are in good agreement with the experimental data. As the lattice constants of AlAs and GaAs are nearly equal and their dielectric constants are very similar it is possible to calculate the effects of structural disorder in AlGaAs lattices based on calculations of a single $Al_{255}GaAs_{256}$ and $AlGa_{255}As_{256}$ supercell. From these calculations the effect of a Ga or Al on a specific As can be calculated and these contributions can be used in an

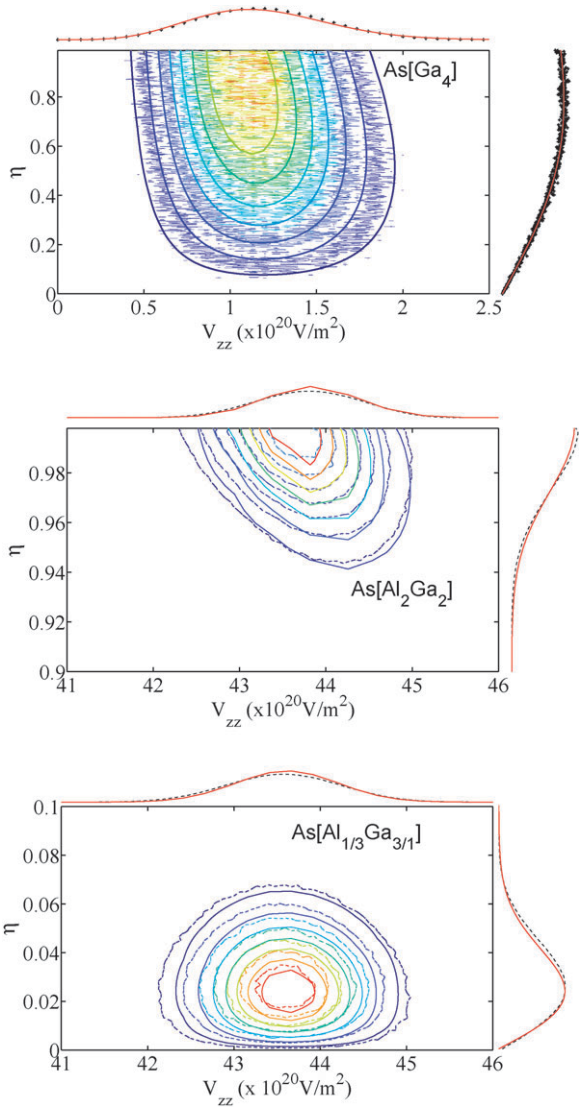

Fig. 13 Overlayed contour plots of the probability density function in quadrupolar coupling parameters $P(V_{zz},\eta)$ generated from DFT calculations and using the analytical expression from Czjzek[25] and Le Caer and Brand.[26] The dotted lines are the DFT-derived data using the multipole model for $S = 0$ of As[Ga_4] (more noisy lines, top plot), As[Al_2Ga_2] (middle) and As[Al_1Ga_3]/As[Al_3Ga_1] (bottom). The solid lines show the Czjzek distribution with an average field gradient of 1.19×10^{20} V m^{-2} and $d = 5$ (top), the extended Czjzek distribution and a first shell tensor $V^{\eta 1} = 33.1$ MHz, $\eta(0) = 1$ (middle) and $V^{\eta 0} = 33.1$ MHz $\eta(0) = 0$ (bottom). All DFT calculations are based on the "Ga in sea of Al" approach.

additive manner when generating large numbers of random or partly ordered structures. The distribution in quadrupolar parameters of the As sites derived from these analyses for randomly ordered materials perfectly match those from the Czjzek (Gaussian isotropic) models used to describe the experimental data. The Ga DFT simulations for $S = 0$ nearly match a Czjzek type distribution with $d = 5$, but the distribution is more complex. In general the calculations predict a shift and narrowing of the distribution in quadrupolar coupling constant with increasing order parameter. Furthermore the calculations show that there is an influence on the local EFG

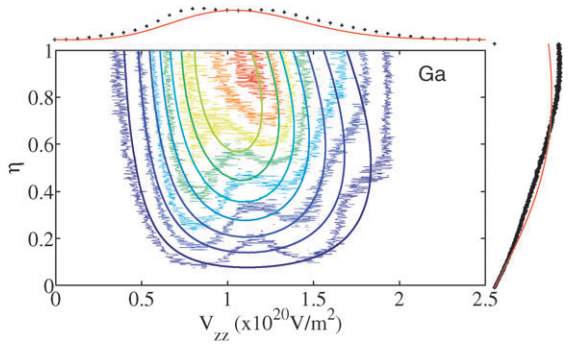

Fig. 14 Simulated probability density function in the quadrupolar parameters of gallium, for $S = 0$ in a $Al_{0.5}Ga_{0.5}As$ lattice. The solid lines show a Czjzek distribution with $\sigma = 230$ kHz and $d = 5$ for ^{69}Ga.

up to the 7th coordination shell, with the first three shells being most dominant.

Our findings of random cation arrangement for $x \approx 0.297$ and $x \approx 0.489$ agrees with earlier studies. Degen *et al.* found a short-range parameter $S \sim 0$–0.2 for similar samples on the bases of the intensities of the two symmetric As sites, with $n = 0,4$. Most studies of long-range order in these semiconductors claim that the order parameter is quite small $S < 0.05$, indicating that clusters of similar ordering are not linked throughout the entire sample. Our data do not fit very well using a long-range order parameter model even for $S = 0$. This might indicate that some short range order exists. Indeed, long and short-range order parameters do not have to be in the same range. Interrupted Al/Ga strings are observed in AlGaAs in an XSTM study.[10] They find a volume fraction of Al strings of only $\sim$0.3% for $x = 0.15$. The presence of Al strings would be observed in our resolved ^{75}As spectra, if the volume fraction of strings is sufficient, roughly >1%. Besides sensitivity, an additional problem for analyzing powdered NMR data is that the distribution in EFG is convoluted with the powder distribution. The EFG tensors of the As[Al_nGa_{1-n}], $n = 1,2,3$ sites have distinct orientations which are modulated by specific order or disorder in the higher coordination shell. Therefore more subtle studies of potential local order in these materials would require the possibility to study a single oriented film, which demands a further increase in volume sensitivity. Miniaturization is a key concept here. We have recently shown advances in this area, using stripline based micro-coil detectors.[14]

Acknowledgements

The authors would like to thank J. van Os and G. Janssen for technical support; M. Voncken for providing the AlGaAs samples; A. Lipton for his assistance on the Simpson discussion forum; A. Brinkmann and R. Siegel for experimental help and for the assistance with SIMPSON; C. Degen for aiding with the formulas to determine the intensities of the sites and S. Vasa for stimulating discussions. The DFT study is part of the research program of the "Stichting voor Fundamenteel Onderzoek der Materie (FOM)". Financial support from the Nederlandse Organisatie voor Wetenschappelijk Onderzoek (Netherlands Organization for Scientific Research, NWO) is

Table 5 EFG simulations of $Al_{0.5}Ga_{0.5}As$ compared to experimental results from Degen *et al.*[21] and to the results of this study. The numbers A(*C*)*n* represent A = average C_q value in MHz, *C* = standard deviation of the distribution in MHz, *n* = number of occurrences in the model. ($C/\sqrt{n}$ represents the accuracy of the mean value in MHz), "—" non-existing entries. The DFT calculations for the super cell models were carried out in a 2 × 2 × 2 unit cell, with 32 arsenic, and a total of 32 (aluminium and gallium) atoms. 10 super cells were used for $x = 0.5$

	Theory ($x = 0.5$)			Experiment ($x \approx 0.489$)	
	Ordered CuAu $S = 1$	Supercell models $S \sim 0$	Multipole model $S = 0$	Single value fit[21]	This study
C_q(MHz)					
^{69}Ga	0.20 (0) 16	0.54 (0.20) 160	0.46	0.52 ± 0.02	
Al	0.046 (0) 16	0.16 (0.06) 160	0.18	0.083 ± 0.007	
As[Ga_4]	—	0.71 (0.23) 17	0.40[c]	0.61 ± 0.020	0.61[ac]
As[Al_4]	—	1.07 (0.33) 14	0.42[c]	0.82 ± 0.050	0.82[ac]
As[$Al_{1/3}Ga_{3/1}$]	—	32.90 (0.59) 176	33.0[ec]	>9	33.3 ± 0.1[ec]
As[Al_2Ga_2]	34.7 (0) 32	33.20 (3.07) 113	33.1[ec]	>9	32.5 ± 0.1[ec]
η					
^{69}Ga	0	0.62 (0.25)	0.63	>0.97	
Al	0	0.57 (0.28)	0.64	>0.96	
As[Ga_4]	—	0.63 (0.21)	0.61	>0.97	0.66
As[Al_4]	—	0.66 (0.28)	0.61	>0.88	0.66
As[$Al_{1/3}Ga_{3/1}$]	—	0.03 (0.02)	0.03		0.03
As[Al_2Ga_2]	0.93 (0)	0.94 (0.02)	0.98		0.98

[c] Czjzek distribution with $\langle C_q \rangle = 2.0 \cdot \sigma$ for $d = 5$; [ac] Assumed Czjzek distribution with $d = 5$ and C_q from the nutation data from ref. 21; [ec] Extended Czjzek distribution. Note that the compared values are average EFGs and not first shell EFGs, although they do not differ much.

Table 6 EFG simulations of $Al_{0.3}Ga_{0.7}As$ compared to the experimental results. The left column displays the results from a single simulation with the highest ordering, the second column displays the result from 3 partially ordered simulations, the third column from 11 random simulations

	Theory ($x = 0.3125$)			
	Ordered CuAu $S_{CuAu} = 0.375$	Part. ord. $S_{CuAu} = 0.125$	Supercell models $S \sim 0$	Experiment ($x \approx 0.297$)
C_q (MHz)				
^{69}Ga	0.54 (0.14) 22	0.47 (0.19) 66	0.45 (0.20) 242	0.69 ± 0.10[m]
^{27}Al	0.14 (0.06) 10	0.09 (0.05) 30	0.14 (0.06) 110	
As[Ga_4]	0.81 (0.35) 12	0.75 (0.25) 28	0.89 (0.29) 68	0.61[ac]
As[$Al_{1/3}Ga_{3/1}$]	33.1 (0.27) 8	33.1 (0.37) 24	32.97 (0.55) 180	33.2 ± 0.1[ec]
As[Al_2Ga_2]	34.5 (0.71) 12	34.6 (0.74) 44	33.36 (0.75) 102	30.3 ± 0.1[ec]
η				
Ga	0.62 (0.30)	0.71 (0.26)	0.61 (0.25)	0.67
Al	0.40 (0.25)	0.22 (0.27)	0.55 (0.28)	
As[Ga_4]	0.47 (0.26)	0.43 (0.23)	0.61 (0.23)	0.67
As[$Al_{1/3}Ga_{3/1}$]	0.04 (0.02)	0.03 (0.02)	0.03 (0.02)	0.03
As[Al_2Ga_2]	0.90 (0.03)	0.90 (0.03)	0.94 (0.02)	0.98

[m] MQMAS and nutation. [ec] Extended Czjzek distribution.

acknowledged for sponsoring the solid-state NMR facility for advanced materials science where the NMR experiments were performed and the Stichting Nationale Computerfaciliteiten (National Computing Facilities Foundation, NCF) for the use of supercomputer facilities.

References

1 G. P. Srivastava, J. L. Martins and A. Zunger, *Phys. Rev. B: Condens. Matter*, 1985, **31**, 2561–2564.
2 G. B. Stringfellow and G. S. Chen, *J. Vac. Sci. Technol., B*, 1991, **9**, 2182–2188.
3 A. Gomyo, T. Susuki and S. Iijima, *Phys. Rev. Lett.*, 1988, **60**, 2645–2648.
4 S. Froyen, A. Zunger and A. Mascarenhas, *Appl. Phys. Lett.*, 1996, **68**, 2852–2854.
5 C. Krahmer, M. Philippens, M. Schubert and K. Streubel, *J. Cryst. Growth*, 2007, **298**, 18–22.
6 T. S. Kuan, T. F. Kuech and W. I. Wang, *Phys. Rev. Lett.*, 1985, **54**, 201–204.
7 A. van Niftrik, G. Bauhuis and J. J. Schermer, *J. Cryst. Growth*, 2006, **289**, 48–54.
8 A. R. Smith, K. Chao, C. K. Shih, Y. C. Shih and B. G. Streetman, *Appl. Phys. Lett.*, 1994, **64**, 478.
9 A. R. Smith, K. Chao, C. K. Shih, K. A. Anselm, A. Srinivasan and B. G. Streetman, *Appl. Phys. Lett.*, 1996, **69**, 1214–1216.
10 A. Heinrich and M. Wenderoth, *Phys. Rev. B: Condens. Matter Mater. Phys.*, 1999, **59**, 10296–10301.
11 S. Adachi, *Properties of Aluminium Gallium Arsenide*, Institution of Engineering and Technology, 1993.
12 A. P. M. Kentgens, J. J. M. Lemmens, F. M. M. Geurts and W. S. Veeman, *J. Magn. Reson.*, 1987, **71**, 62–74.
13 A. Samoson and E. Lippmaa, *J. Magn. Reson.*, 1988, **79**, 255–268.
14 A. P. M. Kentgens, J. Bart, P. J. M. van Bentum, A. Brinkmann, E. R. H. Van Eck, J. G. E. Gardeniers, J. W. G. Janssen, P. Knijn, S. Vasa and M. H. W. Verkuijlen, *J. Chem. Phys.*, 2008, **128**, 052202.
15 J. A. Tang, J. D. Masuda, T. J. Boyle and R. W. Schurko, *ChemPhysChem*, 2006, **7**, 117–130.
16 F. H. Larsen, I. Farnan and A. S. Lipton, *J. Magn. Reson.*, 2006, **178**, 228–236.

17 F. H. Larsen and N. C. Nielsen, *J. Phys. Chem. A*, 1999, **103**, 10825–10832.
18 F. H. Larsen, H. J. Jakobsen, P. D. Ellis and N. C. Nielsen, *J. Magn. Reson.*, 1998, **131**, 144–147.
19 A. Medek, J. S. Harwood and L. Frydman, *J. Am. Chem. Soc.*, 1995, **117**, 12779–12787.
20 B. D. Cullity, *Elements of X-ray diffraction*, Addison-Wesley, Reading, MA, 2nd edn, 1978.
21 C. Degen, M. Tomaselli, B. H. Meier, M. M. A. J. Voncken and A. P. M. Kentgens, *Phys. Rev. B: Condens. Matter Mater. Phys.*, 2004, **69**, 193303.
22 R. Tycko, G. Dabbaghand, S. R. Kurtz and J. P. Goral, *Phys. Rev. B: Condens. Matter*, 1992, **45**, 13452–13458.
23 C. Jäger, G. Kunath, P. Losso and G. Scheler, *Solid State Nucl. Magn. Reson.*, 1993, **2**, 73–82.
24 R. H. Meinhold, R. C. T. Slade and R. H. Newman, *Appl. Magn. Reson.*, 1993, **4**, 121–140.
25 G. Czjzek, J. Fink, F. Gotz, H. Schmidt, J. M. D. Coey, J. P. Rebouillat and A. Lienard, *Phys. Rev. B: Condens. Matter*, 1981, **23**, 2513–2530.
26 G. Le Caër and R. A. Brand, *J. Phys.: Condens. Matter*, 1998, **10**, 10715–10774.
27 H. J. Stöckmann, *J. Magn. Reson.*, 1981, **44**, 145–158.
28 J.-B. d'Espinose de lacaillerie, C. Fretigny and D. Massiot, *J. Magn. Reson.*, 2008, **192**, 244–251.
29 G. Le Caër, B. Bureau and D. Massiot, *J. Phys.: Condens. Matter*, 2010, **22**, 065402.
30 P. Blaha, K. Schwarz and P. Herzig, *Phys. Rev. Lett.*, 1985, **54**, 1192.
31 H. M. Petrilli, P. E. Blöchl, P. Blaha and K. Schwarz, *Phys. Rev. B: Condens. Matter Mater. Phys.*, 1998, **57**, 14690.
32 G. Kresse and J. Hafner, *Phys. Rev. B: Condens. Matter*, 1993, **47**, 558.
33 G. Kresse and J. Hafner, *Phys. Rev. B: Condens. Matter*, 1994, **49**, 14251.
34 G. Kresse and F. J., *Comput. Mater. Sci.*, 1996, **6**, 15.
35 G. Kresse and F. J., *Phys. Rev. B: Condens. Matter*, 1996, **54**, 11169.
36 E. Yablonovitch, T. Gmitter and J. P. Harbison, *Appl. Phys. Lett.*, 1987, **51**, 2222–2224.
37 M. E. Smith and E. R. H. van Eck, *Prog. Nucl. Magn. Reson. Spectrosc.*, 1999, **34**, 159–201.
38 W. L. Meerts and M. Schmitt, *Int. Rev. Phys. Chem.*, 2006, **25**, 353–406.
39 M. Bak, J. T. Rasmussen and N. Nielsen, *J. Magn. Reson.*, 2000, **147**, 296–330.
40 T. Vosegaard, A. Malmendal and N. C. Nielsen, *Monatsh. Chem.*, 2002, **133**, 1555–1574.
41 P. E. Blöchl, *Phys. Rev. B: Condens. Matter*, 1994, **50**, 17953.
42 G. Kresse and D. Joubert, *Phys. Rev. B: Condens. Matter Mater. Phys.*, 1999, **59**, 1758.
43 DALTON, a molecular electronic structure program, Release 2.0 (2005), see http://www.kjemi.uio.no/software/dalton/dalton.html.
44 J. P. Perdew, K. Burke and M. Ernzerhof, *Phys. Rev. Lett.*, 1996, **77**, 3865.
45 C. Degen, *PhD thesis*, ETH Zurich, 2005.
46 G. Engelhardt and H. Koller, *Magn. Reson. Chem.*, 1991, **29**, 941–945.
47 O. H. Han, H. K. C. Timken and E. Oldfield, *J. Chem. Phys.*, 1988, **89**, 6046.
48 A. P. M. Kentgens, *Geoderma*, 1997, **80**, 271–306.
49 S. Wei and A. Zunger, *J. Chem. Phys.*, 1997, **107**, 1931–1935.
50 Z. H. Levine and D. C. Allan, *Phys. Rev. Lett.*, 1991, **66**, 41–44.